DELFT UNIVERSITY OF TECHNOLOGY

MASTER THESIS

Characterisation of Surfactant Polymer Oil Bank Mobilisation Through Relative Permeability Analysis

Author:
Maxim WIJSMAN

Supervisors:
Prof. Ir. Cor VAN KRUIJSDIJK
Dr. Karl-Heinz WOLF

A thesis submitted in fulfillment of the requirements for the degree of ***Master of Science***

in

Applied Earth Sciences
Petroleum Engineering Track

to be defended publicly on
Wednesday March 21, 2018

Declaration of Authorship

I, Maxim WIJSMAN, declare that this thesis titled, "Characterisation of Surfactant Polymer Oil Bank Mobilisation Through Relative Permeability Analysis" and the work presented in it are my own. I confirm that:

- This work was done wholly or mainly while in candidature for a research degree at this University.
- Where any part of this thesis has previously been submitted for a degree or any other qualification at this University or any other institution, this has been clearly stated.
- Where I have consulted the published work of others, this is always clearly attributed.
- Where I have quoted from the work of others, the source is always given. With the exception of such quotations, this thesis is entirely my own work.
- I have acknowledged all main sources of help.
- Where the thesis is based on work done by myself jointly with others, I have made clear exactly what was done by others and what I have contributed myself.

Signed: _____

Date: _____

"A problem worthy of attack proves its worth by fighting back."

Piet Hein

DELFT UNIVERSITY OF TECHNOLOGY

Abstract

Civil Engineering & Geosciences
Applied Earth Sciences

Master of Science

Characterisation of Surfactant Polymer Oil Bank Mobilisation Through Relative Permeability Analysis

by Maxim WIJSMAN

This research project attempts to improve the understanding of oil bank formation in Fontainebleau sandstone cores using a surfactant polymer (SP) EOR method. While oil bank formation is generally successful in longer length cores, it is elusive in short cores (<10cm). Core flooding experiments were performed in a specially designed setup allowing tests to be done on cores with varying length and rock properties. The cores were saturated with a model oil, dodecane, and the injected surfactant polymer slug was optimised using phase behaviour testing. The first objective was to see whether the chosen SP could efficiently mobilise the residual oil left after water flooding and create an oil bank. This was successful in the 17 and 30cm cores as expected, the tests were also successful for the shorter (7cm) cores. A small amount of tests were also done under a CT-scanner. Using iododecane as the dopant, the displacement of oil was visualised at regular intervals during the flooding stages. The images confirm oil bank formation and also gave insight into the rock properties. Although the cores were chosen for its homogeneous properties, many of the cores showed fingering and two layer displacement which would indicate otherwise. Recovery factors averaged around 80% for the low permeability cores and up to 90% for the higher permeabilities. Production data was the main source of output data and subjected to various methods of analysis with a focus on effective relative permeabilities. Using the analytical JBN approach which is normally applied on waterflood data, this relatively simple method was tested to see whether it could produce accurate relative permeability curves which are essential to EOR analysis. Current standard practice involves matching pressure and production data which is both complex and time consuming. The resulting relative permeabilities show that under identical displacement processes the surfactant polymer mobilises oil more freely in cores with higher pore volume. The results from the JBN method were compared to results using Shell's in-house numerical simulator (MoReS). For most core lengths the results from the simulator confirmed the relative permeability curves obtained using the JBN method. In the experiments with large discrepancies further studies should be done to determine whether this was caused by an error in the method or by the heterogeneities in the cores as seen on the CT scan. Using this approach could offer an efficient and robust alternative to the current technique of establishing RelPerm curves.

Acknowledgements

Spending almost a year on a research project undoubtedly brought with it its fair share of challenges and setbacks. These were not only scientific in nature but also personal. Overcoming these made bringing together all of the results, observations and experiences especially rewarding. Getting to this point would not have been possible without the knowledge and support of a number of people who deserve to be mentioned.

First of all Faisal, you were exactly what any MSc student hopes for in a thesis supervisor. From the start of the project you were able to keep the perfect balance of support and independence, letting me learn the experimental procedures "by doing" rather than having me watch from the sidelines first. Whenever I did run into issues you never hesitated to help, even on weekends or while you were on holiday. Lastly I'd like to thank you for giving me the chance to experience what it is like to work at the Shell Offices and for introducing me to the people working there, many of which will be mentioned here for their contributions.

Secondly I would like to thank Cor for being something of a beacon in the fog that a large research project like this can be. Sometimes it is hard to keep track of the big picture when you are in the thick of it. You were always able to focus our efforts into the right direction. The same can be said for Karl-Heinz, also thank you for keeping me on my toes and safe during the months I spent in the laboratory.

Speaking of the laboratory, thank you to Michiel for helping me keep the set-up up and running, and spending days in CT room trying to get the one meter core flood working. A very big thank you to Ellen Meijvogel, Karel Heller, Jolanda van Haagen-Donker, Marc Friebel, Joost van Meel, Wim Verwaal, Martijn Jannsen and Jens van den Berg. I would also like to thank everyone in the Rock and Fluid Physics team at Shell. A special mention for Merit van der Lee, Steffen Berg, Diederik van Batenburg, Xuesong Li, Hilbert van der Linde, Efraim Keijzer and Jasper de Reus for your help with the experimental procedures and interpretation of the resulting data.

Finally a warm thank you to my parents, family and all my friends for the welcomed support and distractions over the past year.

Maxim Wijsman
Delft, March 2018

Contents

Declaration of Authorship iii

Abstract vii

Acknowledgements ix

1 Introduction 1
1.1 . . . 1

2 Theory 3
2.1 Concepts of Surfactant Polymer Flooding . . . 3
2.1.1 Darcy's Law . . . 3
2.1.2 Mobility . . . 4
2.1.3 Interfacial Tension . . . 4
2.1.4 Wettability . . . 4
2.2 Oil Bank Mobilisation . . . 5
2.2.1 Mobilising Residual Oil . . . 5
2.3 EOR Chemicals . . . 6
2.3.1 Surfactant . . . 6
2.3.2 Microemulsions . . . 6
2.3.3 Phase Behaviour . . . 7
2.3.4 Co-solvent . . . 8
2.3.5 Polymer . . . 9
2.4 Flooding Analysis . . . 9
2.4.1 JBN Method . . . 9
2.4.2 Numerical Simulation . . . 10
2.4.3 Tracer Analysis . . . 10

3 Experimental Design 13
3.1 Phase Behaviour Screening . . . 13
3.1.1 Chemical EOR Fluids . . . 13
Surfactant . . . 13
Co-Solvent . . . 14
Surfactant System . . . 14
Oil . . . 14
Polymer & Viscosity Measurements . . . 14
3.1.2 Methodology . . . 15
Salinity Scan . . . 15
IFT Measurements . . . 15
3.2 Core Flooding Experiments . . . 16
3.2.1 Equipment . . . 16
Core Flood Setup . . . 16
Fontainebleau Cores . . . 17

CT Scanner . . . 17
3.2.2 Methodology . . . 18
3.2.3 Tracer Analysis . . . 18

4 Phase Behaviour Analysis **21**
4.1 Phase Behaviour . . . 21
Dodecane . . . 21
Iodododecane . . . 21
Co-Solvent Concentration . . . 22
4.2 IFT Measurements . . . 22
Optimum . . . 23
Underoptimum . . . 23

5 Results: Core Flood **25**
5.1 17cm Low Permeability . . . 25
5.1.1 CT Scan . . . 25
Oil Saturation & Waterflood . . . 25
Surfactant Polymer . . . 26
5.1.2 Production Data . . . 27
Waterflood . . . 28
Chemical Flood . . . 28
Pressure Response . . . 28
5.1.3 Non-CT Production Data . . . 29
5.2 39cm Low Permeability . . . 30
5.2.1 CT Scan . . . 30
5.2.2 Production Data . . . 31
5.2.3 Non-CT Production Data . . . 32
5.3 7cm High Permeability . . . 32
5.3.1 Production Data . . . 32
5.4 17cm High Permeability . . . 33
5.4.1 Production Data . . . 33
5.5 30cm High Permeability . . . 34
5.5.1 CT Results . . . 34
CT Production Data . . . 35
5.5.2 Production data . . . 35
5.6 Discussion . . . 36
5.6.1 Reproducibility . . . 36
5.6.2 Decreased Surfactant Polymer Slug Size . . . 37
5.6.3 Underoptimum Injection Conditions . . . 37

6 Results: Analytical JBN Method **39**
6.1 17cm Low Permeability . . . 39
6.2 39cm Low Permeability . . . 40
6.3 7cm High Permeability . . . 42
6.4 17cm High Permeability . . . 42
6.5 30cm High Permeability . . . 44
6.6 Discussion . . . 45
6.6.1 Low Permeability 17 vs 39cm . . . 45
6.6.2 High Permeability 7 vs 17cm vs 39cm . . . 45
6.6.3 High vs. Low Permeability . . . 46

7 Results: Numerical Simulator **49**
7.1 Atlas 23 . . . 49
7.1.1 17cm Low Permeability . . . 49
7.1.2 39cm Low Permeability . . . 51
7.1.3 7cm High Permeability . . . 52
7.1.4 17cm High Permeability . . . 52
7.2 Atlas 53 . . . 54
7.2.1 17cm Low Permeability . . . 55
7.2.2 7cm High Permeability . . . 57
7.2.3 17cm High Permeability . . . 58

8 Conclusions **59**

9 Recommendations **61**

A Phase Behaviour **63**

B Surfactant-Polymer Viscosities **65**

C Tracer Analysis **67**

D Pressure Data - 30cm Chemical Flood **69**

E Analysis - 1m Low Perm. Cores **71**

Bibliography **73**

List of Figures

2.1 Capillary Desaturation Curve . . . 5
2.2 Critical Micelle Concentration . . . 7
2.3 Phase Behaviour . . . 8

3.1 Surfactant Structure . . . 13
3.2 Spinning Drop Method . . . 15
3.3 Coreflood Schematic . . . 16
3.4 Coreflood Setup . . . 17

4.1 Dodecane Salinity Scan . . . 22
4.2 IFT Dodecane . . . 23

5.1 Oil Saturation . . . 25
5.2 CT Waterflood . . . 26
5.3 CT Surfactant Polymer . . . 26
5.4 17cm Production Data . . . 27
5.5 17cm Pressure Data . . . 28
5.6 17cm Production Data . . . 29
5.7 39cm Chemical Flood CT . . . 30
5.8 39cm CT Production Data . . . 31
5.9 7cm Production Data . . . 32
5.10 17cm HP Production Data . . . 33
5.11 30cm HP Fingering . . . 34
5.12 30cm HP CT . . . 34
5.13 30cm CT HP Production . . . 35
5.14 Reproducibility 17cm HP . . . 36
5.15 Reproducibility 30cm HP . . . 37
5.16 Core Flood Results Summary . . . 38

6.1 JBN - 17cm Low Perm . . . 39
6.2 JBN - Reproducibility . . . 40
6.3 JBN - 39cm Low Perm . . . 41
6.4 JBN - 7cm High Perm . . . 42
6.5 JBN - 17cm High Perm . . . 43
6.6 JBN - 30cm High Perm . . . 44
6.7 JBN - 17 vs 39cm . . . 45
6.8 JBN - 7vs17vs39cm . . . 46
6.9 JBN - 17cm High vs Low Perm . . . 47

7.1 Atlas 23 - 2D Simulator Grid . . . 50
7.2 Atlas 23 - 17cm LP . . . 51
7.3 Atlas 23 - 39cm LP . . . 51
7.4 Atlas 23 - 7cm HP . . . 52
7.5 Atlas 23 - 17cm HP . . . 53

7.6 Atlas 53 - Grid 54
7.7 Atlas 53 - Chemical Flood 55
7.8 Atlas 53 - 17cm Low Perm 56
7.9 Atlas 53 - 17cm Pressure 56
7.10 Atlas 53 - 7cm Low Perm 57
7.11 Atlas 53 - 7cm Chemical Flood 57
7.12 Atlas 53 - 9cm Low Perm 58

A.1 Iodododecane Salinity Scan 63
A.2 Equilibration 64

B.1 Rheometer Results 66

C.1 Tracer Results 67

D.1 30cm CT Pressure Results 69

E.1 1m Low Permeability Core Analysis 72

List of Tables

3.1 Preliminary surfactant compositions 14
3.2 Properties of the oils used 14

4.1 Optimum Salinity 21

List of Abbreviations

EOR	**E**nhanced **O**il **R**ecovery
OIIP	**O**il **I**nitially **I**n **P**lace
IFT	**I**nter**f**acial **T**ension
IPA	**I**so**p**ropyl **A**lcohol
IOS	**I**nternal **O**lefin **S**urfactant
CMC	**C**ritical **M**icelle **C**oncentration
HPAM	**H**ydrolysed **P**oly**a**crila**m**ides
RPM	**R**ounds **P**er **M**inute
FB	**F**ontaine**b**leu
CT	**C**omputed **T**omography
PV	**P**ore **V**olume
SBA	**S**econd **B**ut**a**nol
SP	**S**urfactant **P**olymer
WF	**W**ater **F**lood
HP	**H**igh **P**ermeability
LP	**L**ow **P**ermeability

List of Symbols

N_c	capillary number	
N_b	bond number	
$k_{r\alpha}$	relative permeability	
λ	mobility	
I_r	relative injectivity	
f_α	fractional flow of phase α	
S_α	saturation of phase α	
u	superficial velocity	$\mathrm{m\,s^{-1}}$
k	permeability	$\mathrm{m^2}$
μ	viscosity	$\mathrm{m^2\,s^{-1}}$
$\nabla\Phi$	pressure gradient vector	$\mathrm{Pa\,m^{-1}}$
P_c	capillary Pressure	Pa
γ	interfacial tension	$\mathrm{N\,m^{-1}}$
C	concentration	$\mathrm{mol\,m^{-3}}$

Chapter 1

Introduction

1.1

Global energy consumption will continue to rise unremittingly and although crude oil will undoubtedly lose some of its market share, absolute crude oil consumption is expected to rise for the next two decades (BP, 2018). Due to the down-cycle in the energy industry and a surge in shale production, new hydrocarbon discoveries reached a 5-year low in 2017. Given the capital- and time-intensive nature of developing a new field, existing fields will be looked upon when supply begins to fall short of demand. Enhanced oil recovery (EOR) is a collection of technologies that allow operating companies to produce incremental oil from fields that are well into their production life cycle. At this point the field has most likely undergone secondary oil recovery (water injection for pressure maintenance and oil mobilisation) however it will still contain approximately 60-80% of the oil initially in place (OIIP).

This remaining oil is comprised of oil ganglion dispersed in the reservoir pores plus bypassed oil which has not seen injection water. This trapping occurs because the capillary forces exceed the viscous forces exerted by the displacing fluid, usually brine. Mobilising the remaining oil involves improving the sweep efficiency or increasing the capillary number (N_c); this can be done by by increasing the viscosity of the displacing fluid, or by lowering the interfacial tension (IFT) between the two phases, respectively. Surfactant polymer injection aims to do both of these.

Surfactant addition is one of the fundamental mechanisms in chemical EOR. By injecting these compounds into the reservoir the IFT of the oil/water interface decreases significantly. Since the effectiveness of the surfactant is largely salinity dependent, the formulation must be optimised to ensure that the resulting oil-surfactant microemulsions exhibit the ultra-low IFT's for oil mobilisation.

Once injected the surfactant polymer will attempt to mobilise the dispersed oil droplet, if successful these will begin to propagate ahead of the front. As more and more oil is mobilised the droplets will converge to form a coherent oil body, also known as an oil bank. In a field the production of such an oil bank is the most economically advantageous method of producing residual oil since it requires minimal processing.

This research project attempts to recreate oil bank formation using an experimental coreflood set-up. An initially oil-saturated core first undergoes waterflooding and is then flooded with the optimised surfactant polymer solution. Production data and a CT scanner allows flow-analysis to be done on the displacement processes. Using cores of different lengths and properties the different experiments were compared using relative permeabilities, to determine what factors characterise the mobilisation of the oil bank.

Chapter 2

Theory

2.1 Concepts of Surfactant Polymer Flooding

To understand and analyse the processes and characteristics of the core flooding experiments in this research project, some fundamental concepts will be briefly discussed.

2.1.1 Darcy's Law

The experiments and simulations performed for this research all try to model the flow of fluid through a medium of interconnected pores. Henry Darcy described this flow based on the viscosity (μ) of the fluid, the pore geometry and interconnectedness of the matrix (k), and the driving force or flow potential (Φ). The resulting superficial velocity is given by Darcy's law.

$$\vec{u} = -\frac{k}{\mu} \cdot \nabla\Phi \tag{2.1}$$

Originally derived for single-phase, laminar flow; the latter should be acceptable since flow in a reservoir only occurs in a range of low Reynold's numbers (Holmes et al., 2016). However when applying the equation to multi-phase flow the capillary pressure between the two phases will complicate things. The flow of each phase will be influenced by local pressure disturbances due to the respective saturation at that point. Percolation aspects further reduce the permeability of each phase since the presence of two phases lowers both their respective connectivity. This makes it necessary to introduce a distinction between the two, known as relative permeability.

$$\vec{u_w} = -\frac{\vec{k} \cdot k_{rw}(S_w)}{\mu_w} \cdot \nabla\Phi_w \tag{2.2}$$

$$\vec{u_o} = -\frac{\vec{k} \cdot k_{ro}(S_o)}{\mu_o} \cdot \nabla\Phi_o \tag{2.3}$$

$$P_c = p_o + p_w \tag{2.4}$$

In the previous equations $\vec{k} \cdot k_{ro}$ is also known as the effective permeability (k_e). It is the product of the intrinsic permeability of the rock and the relative permeability of the phase. The saturation of the flowing fluid is the dominant parameter and it is therefore often plotted against it, however relative permeability is also a function of the rock properties, absolute permeability, fluid properties, pressure and temperature (Zolotukhin and Ursin, 2000).

2.1.2 Mobility

Using the concept of permeability we can continue by defining the **mobility** of the phase. This is the ratio between the effective permeability and the phase viscosity.

$$\lambda_i = \frac{k \cdot k_{ri}(S_i)}{\mu_i} \tag{2.5}$$

Mobility becomes very interesting when comparing the mobility in front and behind a displacing front. This ratio, known as the **mobility ratio** indicates whether or not the displacement will occur stably or not. A mobility ratio less than one is considered favourable, while a ratio greater than one is unfavourable and means the displacing fluid will have the tendency to bypass or "finger" through the displaced fluid.

2.1.3 Interfacial Tension

Interfacial Tension is the force per unit length parallel to the interface i.e., perpendicular to the local density or concentration gradient (Homsy, 1988). In thermodynamics it is often referred to as the excess free energy per unit area. This excess energy comes from an imbalance in forces due to molecules interacting at the interface. Although dependent on the intrinsic properties of the two phases, the IFT can be influenced by temperature, salinity and surface active agents also known as surfactants.

Methods which measure the IFT all rely on the Young-Laplace equation. This equation describes the capillary pressure difference incurred at the interface and relates this to the shape of the interface

$$\Delta P = -2\gamma H \tag{2.6}$$

This relationship is fundamental to many of the common measuring techniques such as the sessile bubble, pendant bubble and spinning drop method.

2.1.4 Wettability

When placing a fluid near a solid surface in the presence of other immiscible fluids, the degree to which it will adhere to said surface depends on the **wettability**. The adhesive and cohesive forces which determine the wettability are a result of the rock properties, saturation history, fluid composition, temperature and salinity. It is an important characteristic which often dictates the distribution and volume of residual oil (Goddard, 1989). The wettability can be observed in the degree of deformation at the three phase contact point. Thomas Young was the first to quantify this effect by measuring the contact angle of a phase on an ideal surface.

$$\gamma_{ow} cos\theta = \gamma_{os} - \gamma_{ws} \tag{2.7}$$

His equation 2.7 postulated that this angle was related to the interfacial tension between the liquids (γ_{ow}) and the surface energies of the two phases with the substrate (γos, γos).

2.2 Oil Bank Mobilisation

2.2.1 Mobilising Residual Oil

The problem that is faced by all reservoirs during hydrocarbon recovery is the constant interaction between interfacial and viscous forces. It was found that the ratio between these two could be expressed as a dimensionless term known as the capillary number (N_c) (Brownell and Katz, 1947).In some cases the density difference between the phases means that buoyancy forces must also be accounted for in the net force on the trapped phase (Morrow and Songkran, 1981), this is done via the Bond number (N_b). The two formulas read as followed:

$$N_c = \frac{k \cdot \nabla\Phi}{\sigma}; N_b = \frac{k \cdot g \cdot \Delta\rho}{\sigma} \tag{2.8}$$

Under primary recovery the natural pressure gradient ($\nabla\ \Phi$) in the reservoir is sufficient to mobilise a portion of the oil in place. Once this source is depleted water flooding can be used to maintain a normal pressure gradient, however at some point a threshold is reached where the capillary forces trapping the residual oil would require an unrealistically high pressure gradient to induce mobilisation. The capillary number for sandstones such as the Fontainebleau used in this research occupy the range of 10^{-6} to 10^{-7} during waterflooding. (Abrams, 1975) showed that it was necessary to increase the capillary number by two to three orders of magnitude to mobilise any marginal oil. Beyond this *critical capillary number* residual oil has been shown to decrease. This can be confirmed by examining the following capillary desaturation curve (Delshad et al., 1986).

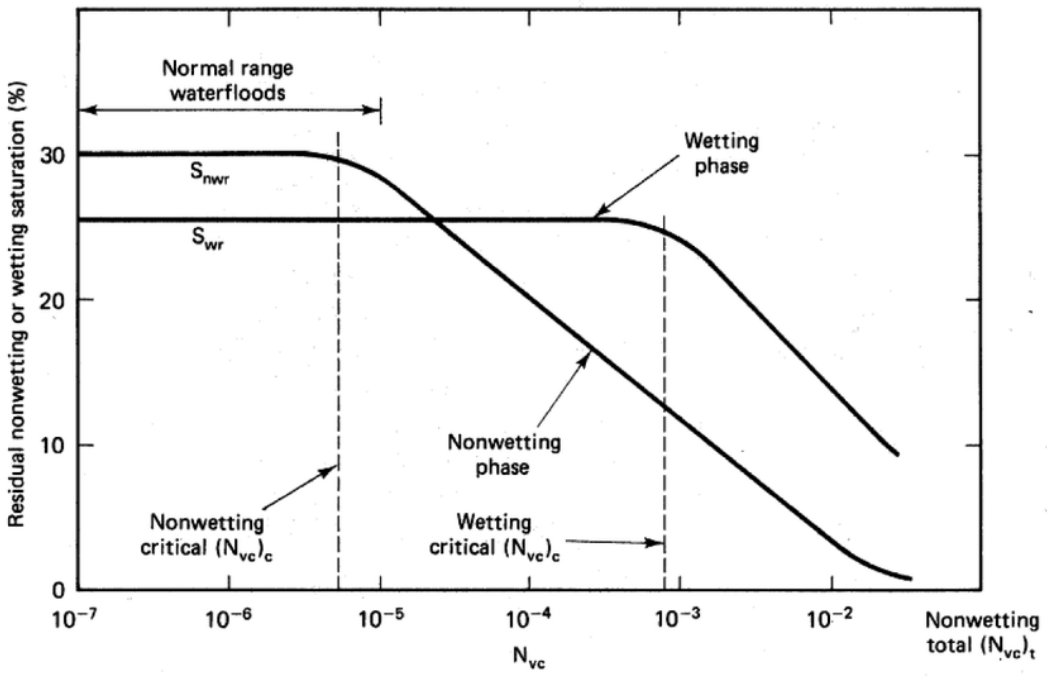

FIGURE 2.1: Capillary Desaturation Curve for a typical sandstone core.

The residual saturations of the wetting and non-wetting phase are relatively constant until the capillary number is high enough. After this the residual saturation of the non-wetting phase begins to decrease first which is in line with the principle of wetting discussed in previous section. Capillary forces can be further reduced by using surfactants to change the oil-water interfacial tension. Rewriting 2.8 using Darcy's law to replace the pressure gradient a common expression for capillary number is obtained.

$$N_c = \frac{\mu \cdot u}{\gamma}; \tag{2.9}$$

Using carefully formulated surfactant solutions the in-situ microemulsions that are formed produce interfacial tensions (γ) in the ultra-low region 10^{-4} dyne/cm. This reduction combined with an increased viscosity due to the polymer increases the capillary number beyond the critical threshold and results in the mobilisation of trapped oil ganglion.

2.3 EOR Chemicals

2.3.1 Surfactant

Surfactants are able to reduce the interfacial tension due to their chemical structure, more specifically their *amphipathic* structure. Each molecule has a hydrophobic head and a hydrophilic tail, placed on opposite ends. This characteristic means that it is energetically favourable for the molecule to sit at the interface rather than in the bulk phase (Miller C, 1986). At the interface the tail of the molecule forms a new interface boundary with a lower dissimilarity in surface energies, resulting in a lower interfacial tension.

Surfactants are classified based on the charge of the hydrophilic group (Rosen and Kunjappu, 2012):

i) *Anionic*: Surfactant ion is negatively charged

ii) *Cationic*: Surfactant ion is positively charged

iii) *Zwitterionic*: Both charges may be present on the surfactant ion

iv) *Nonionic*: Surfactant ion has a neutral charge

The most commonly used of the four categories are the anionic surfactants. When dissolved in water this molecule gives rise to a negatively charged surfactant ion and a positive counter ion. Since many sandstones carry a net negative charge at reservoir conditions (Hirasaki and Zhang, 2004), the degree of adsorption onto the formation is low. Combined with their exceptional performance in lowering the IFT and low cost, these have been the focus of many EOR projects. Examples of commonly used anionic surfactants are *alkylbenzene sulfonates* (ABS), *alcohol ethoxy sulfates* (AES), *alcohol propoxy sulfates* (APS) and *internal olefin sulfonates* (IOS) which will be used in this research.

2.3.2 Microemulsions

One of the mentioned characteristics of surfactants is their preference to accumulate as a monolayer at the interface. However if the surfactant concentration increases

the molecules will begin to aggregate and form structures called **micelles** in the bulk phase. The threshold concentration at which this happens is called the **Critical Micelle Concentration (CMC)**. These structures are chemically interesting because they can trap a volume of a phase depending on the orientation of the surfactant molecules that form the micelle, thereby increasing its solubility.

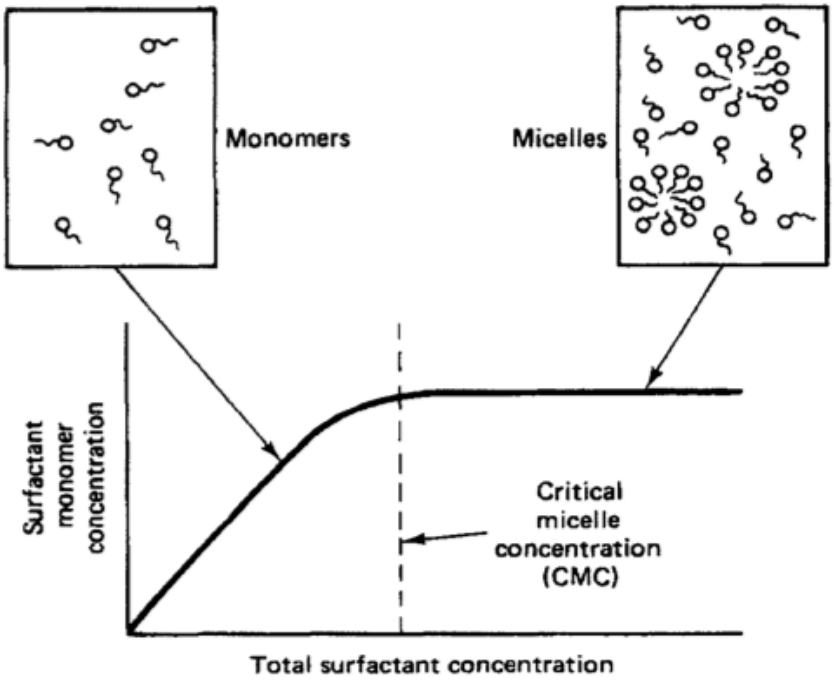

FIGURE 2.2: Illustration of the concept of Critical Micelle Concentration.

Micelles in the water phase will orientate themselves with the hydrophobic tail pointing inwards and trapping a volume of oil inside it. Similarly, micelles in the oil phase will orientate themselves so that more water will be solubized in bulk oil phase. When the micelle concentration is high enough so that large amounts of solubized oil or water is present, the solution is called a **microemulsion**.

The difference between a microemulsion and the more common macroemulsion is that a former is thermodynamically stable (Winsor, 1948). Usually a high interfacial tension will cause the dispersed droplets to coalesce back to their respective phase. The ability of the surfactant molecules to reduce the interfacial tension means that the micelles will cause droplets to disperse spontaneously, thereby creating a microemulsion. The droplet size in a microemulsion is much smaller (100 μm) than its macro- counterpart. This is a reason they are often clear or translucent instead of opaque.

2.3.3 Phase Behaviour

The three phases in a surfactant-oil-brine will interact with each other based on concentrations, composition, temperature, etc. Winsor (1954) was the first to describe this behaviour as **phase behaviour**. He concluded that anionic surfactants were most sensitive to changes in electrolyte concentration, represented by the salinity

of the system. Microemulsions can be categorised using the Winsor classification which looks at the phase preference of the microemulsion.

Winsor *I*: An oil-in-water microemulsion with an excess oil phase on top, also called a lower-phase microemulsion.

Winsor *II*: Higher salinities cause a change in drop curvature leading to a water-in-oil microemulsion. The excess phase is now the brine.

Winsor *III*: A three phase system where similar amounts of oil and brine are solubized and both an excess brine and an excess oil phase are present.

The Type-3 system is of most importance to EOR processes because it exhibits the ultra low interfacial tensions needed to mobilise the residual oil. By varying the salinity the system can be tuned to develop this middle phase. Incrementally increasing the salinity to find the optimum is called a *salinity scan*. Concentrations above and below the optimum salinity are referred to as over- and under-optimum, respectively.

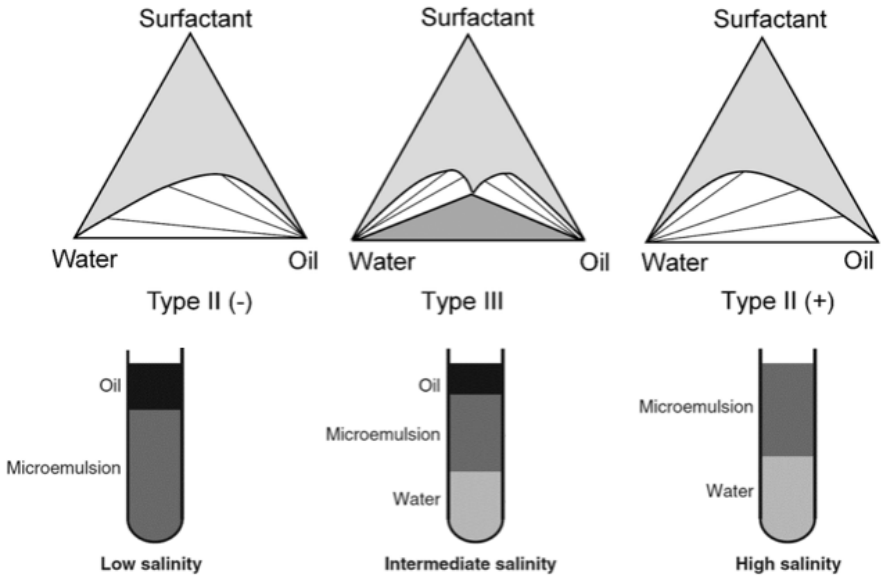

FIGURE 2.3: Winsor classification along with the accompanying ternary diagrams.

2.3.4 Co-solvent

Co-solvents are used to increase the compatibility of the surfactant with the aqueous phase and improve the stability of the solution itself. Ensuring that the all components of the surfactant-polymer slug remain in solution will increase the efficiency of the flood and therefore also the ultimate recovery (Sahni et al., 2010). The co-solvent will reduce any viscous phase and increase the equilibration speed of the microemulsions (Sanz and Pope, 1995). Alcohols are the most commonly used co-solvents and 2-butanol (SBA) will be used in this project.

2.3.5 Polymer

Polymer is added as a means of mobility control. On its own it will not result in any further mobilisation of residual oil, it will however ensure that the mobility ratio of the surfactant front remains low. This means that the slug will sweep the rock more efficiently and prevent viscous fingering (Falls et al., 1994). Polymer can also be used as a chaser slug to achieve a similar result. In this research project polymer is added to the surfactant as well as the chaser slug. This will reduce the impact of unexpected heterogeneities and ensure an optimal sweep of the Fontainebleau cores.

2.4 Flooding Analysis

One of the most telling parameters for multiphase fluid flow and saturation distribution in a reservoir is relative permeability. As mentioned this is the effective permeability of a phase compared to the absolute permeability of the matrix and it is primarily determined through core flooding experiments. This can be done for steady-state (SS) or unsteady-state (USS) experiments. Steady state experiments allow the saturation of the system to equilibrate at different fractional flow ratios. While more accurate this method is time consuming since reaching steady-state can take hours or days. Unsteady-state experiments are time efficient but care must be taken during the analysis to ensure accuracy. To accommodate the large number of experiments done for this research, unsteady-state was most suitable.

2.4.1 JBN Method

One of the most popular unsteady-state methods was chosen to perform the relative permeability analysis, the Johnson, Bossler and Naumann (JBN) method (Johnson, Bossler, and Naumann, 1959). Similar to other methods, JBN builds on top of fractional flow theory (Buckley and Leverett, 1942) and the extended Welge technique (Welge, 1952). The two biggest assumptions for this model to hold true, is that the flow rate must be constant, and high enough to achieve stable displacement. This last requirement can also be met by using mobility control and allows the model to ignore capillary effects.

The input data required for JBN is the differential pressure across the inflow and outflow of the core, as well as the produced volumes of liquids. For the end point relative permeabilities ($K_{ro}S_{wc}$) and ($K_{rw}(1 - S_{or})$, the system is brought to a point where no more oil can be saturated and no more oil can be produced, respectively. At these points the system approaches steady state and Darcy's law can be used. For intermediate relative permeabilities JBN method can be applied in three steps:

All calculations correspond to the outlet of the system since this is where the produced volumes are recorded. First the ratio K_{ro}/K_{rw} is determined. Using fractional flow theory it can be shown that:

$$f_o = \frac{dS_{wav}}{dQ_i} \tag{2.10}$$

Rewriting this using the definition of mobility for each phase 2.5:

$$f_o = \frac{\lambda_o}{\lambda_w + \lambda_o}; \lambda_i = \frac{Kk_{ri}(S_i)}{\mu_i} \tag{2.11}$$

We now have a relationship that includes the ratio between the relative permebailities:

$$f_o = \frac{1}{1 + \frac{K_{ro}}{K_{rw}}} \tag{2.12}$$

Next JBN introduced a term known as the injectivity factor which compares the pressure drop at the current time to the initial value before flooding has commenced.

$$I_r = \frac{\Delta p_i}{\Delta p} \frac{1}{Q_i} \tag{2.13}$$

The oil relative permeability can now be calculated through differentiation involving relative injectivity:

$$K_{ro} = f_o \frac{1}{\frac{d(1/Q_i I_r)}{d(1/Q_i)}} \tag{2.14}$$

Leaving K_{rw} to be defined as:

$$K_{rw} = \frac{(1 - f_o)}{f_o} \frac{\mu_w}{\mu_o} k_{ro} \tag{2.15}$$

Finally the water saturation at the outlet is calculated using the formulation introduced by Welge:

$$S_w = \overline{S_w} - Q_i f_o; \tag{2.16}$$

Using these relationships the normal relative permeability curves can be calculated from unsteady-state data and plotted as a function of water saturation.

2.4.2 Numerical Simulation

The JBN method was originally designed for water flooding experiments. Since in this research project it will be used for chemical flooding data, it is important to have a reference model against which the analytical results can be compared. The first numerical simulator for EOR was developed as early as 1978 (Pope and Nelson, 1978). This was a 1-D simulator which calculated oil recovery as a function of several major variables. Today there are countless commercial reservoir simulators each with their own strengths and weaknesses.

This thesis uses the Modular Reservoir Simulator (MoReS) developed by Shell. It is a comprehensive package and the decks on which the models are built contain many features that are important but also many that are unnecessary for this project. The flexibility of the simulator allows each input to be toggled on or off as desired.

2.4.3 Tracer Analysis

Tracer analysis is built on the theory that over time the mixing of two miscible fluids is dictated by a number of factors. Most important are dispersion and diffusion, while secondary effects include gravity segregation, viscous fingering and stagnant volumes. By adding a tracer chemical to an identical brine solution as what is used in the experiments we can eliminate most of these secondary effects and use a model which defines accessible pore volume as a function of porosity and the dispersion coefficient.

The model used is a 1-D convection-dispersion model as defined by Marle (1981):

$$C = C_I + \frac{C_I - C_J}{2} erf(\frac{x_D - t_D}{2\sqrt{\frac{t_D}{N_{pe}}}}) + \frac{C_I - C_J}{2} erf(\frac{x_D - (t_D - t_{Ds})}{2\sqrt{\frac{(t_D - t_{Ds})}{N_{pe}}}}) \tag{2.17}$$

Here C_I and C_J are the initial and the injected concentration and X_D, t_D, t_{Ds}, are the dimensionless distance, time and injected volumes, respectively.

Chapter 3

Experimental Design

This chapter presents an overview of the materials used and experimental procedures followed in this core flooding project. The experiments can be split up into two distinct steps. The phase behaviour investigation needed to tune the surfactant-oil system to the required specifications is discussed first. Once the system was working optimally the core flooding experiments were carried out, which are described after.

3.1 Phase Behaviour Screening

The optimal phase behaviour was determined by performing a salinity scan on the chosen surfactant formulation. The components and equipment used are listed below followed by the procedure.

3.1.1 Chemical EOR Fluids

Surfactant

Arguably the most important aspect of this research project is the surfactant used to reduce the interfacial and induce oil mobilisation. The surfactant chosen is a tried and tested compound named ENORDET O242, developed by Shell Chemicals. This is an internal olefin surfactant (IOS) that has already seen field application. The structure is built on a hydrophobic carbon chain composed of 20-24 carbon atoms with the active IOS head placed along it (Barnes et al., 2010).

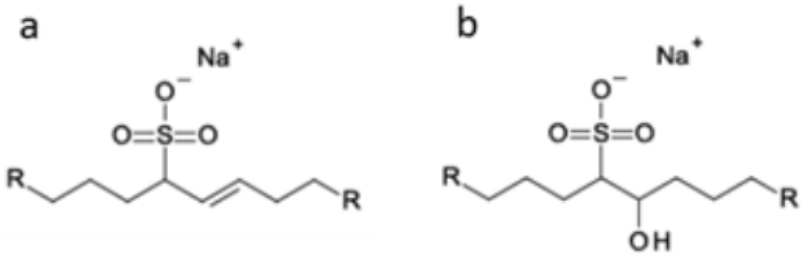

FIGURE 3.1: Chemical structure of the Enordet O242 surfactant. The molecule can either have a double carbon bond or an OH group.

Co-Solvent

As mentioned in the previous chapter the system contains a co-solvent to decrease equilibration time and reduce viscous phase build up, which is problem when using Enordet O242. The chosen co-solvent concentration is 4 wt%, 2-Butanol. This allows for a more flexible interface while still preserving adequate microemulsion volume. At higher concentrations the degree of solubisation becomes too small.

Surfactant System

The composition of the aqueous surfactant solution can then be determined. The table below shows the standard concentrations for the individual components.

TABLE 3.1: Preliminary surfactant compositions

System	Surfactant Conc. (%)	Cosolvent Conc. (%)	Make-up water
I	1	2	Demi Water
II	1	4	Demi Water

The last component of the surfactant solution is the electrolyte sodium chloride. Its concentration will be determined by the optimal salinity in the phase behaviour test.

Oil

The oil used in the experiments is dodecane. It is a refined alkane hydrocarbon that mimics the characteristics of an oleic phase while limiting the amount of secondary interactions. This "ideal" system allows us to study the effect of the surfactant polymer and a greater degree of reproducibility with a limited number of cores. For the experiments in the CT scanner iododododecane was used for its refractive properties.

TABLE 3.2: Properties of the oils used

Name	Formula	Density (kg/m3)	Viscosity (mPa s)
n-Dodecane	C12H26	750	1.34
1-Iododododecane	C12H25I	1200	3.00

Polymer & Viscosity Measurements

The polymer that will be added to the optimum surfactant system is hydrolysed polyacrylamides (HPAM). The stock solution is approximately 3000ppm and will be diluted to achieve a favourable mobility ratio.

Viscosity will be measured using an Anton Paar MCR series rheometer. This is a high precision instrument that will be able to accurately determine the viscosity of the polymer and surfactant-polymer solution. A cup and bob method is used in combination with a constant shear rate test.

3.1.2 Methodology

Salinity Scan

To determine the optimum salinity for the chosen surfactant-oil system a salinity scan was performed. Stock surfactant solution was prepared according to the compositions given in table 3.1. Small quantities of solution were separated and sodium chloride was added incrementally to produce separate batches with increasing salinity. The first series covered a range of 1-5wt% in unit steps. Once properly mixed 10ml of each solution was added to a graduated test tube together with 10ml of dodecane (1:1 volume ratio). The test tubes were shaken vigorously for 60 seconds to accelerate microemulsion formation. The samples were placed in a rack and left to equilibrate under observation. A photo was taken and analysed to determine solubisation ratios and determine optimum salinity. The test was repeated once an approximate optimum salinity was known. The increments in salinity were decreased (steps of 0.25%) to get a more accurate measurement of the optimum. This procedure was carried out for both dodecane and iodododecane.

IFT Measurements

Although it can be assumed that the optimum salinity also exhibits the lowest interfacial tension, it can be tested using a spinning drop tensiometer. The model used was an SVT 20 produced by Dataphysics. Its range is advertised as $1e^{-6}$ to $2e^{3}mN/m$ which should be enough to capture the ultra-low IFT's of the surfactant microemulsions. The device uses the density discrepancy between the two phases and centrifugal force to measure the low IFT's resulting from the surfactant. A capillary tube is filled with the denser phase (brine when using dodecane; oil when using iodododecane), and a drop of the less dense phase is added. By rotating at high RPM's the drop will start to elongate due to the centrifugal force towards the tube walls as seen in figure 3.2.

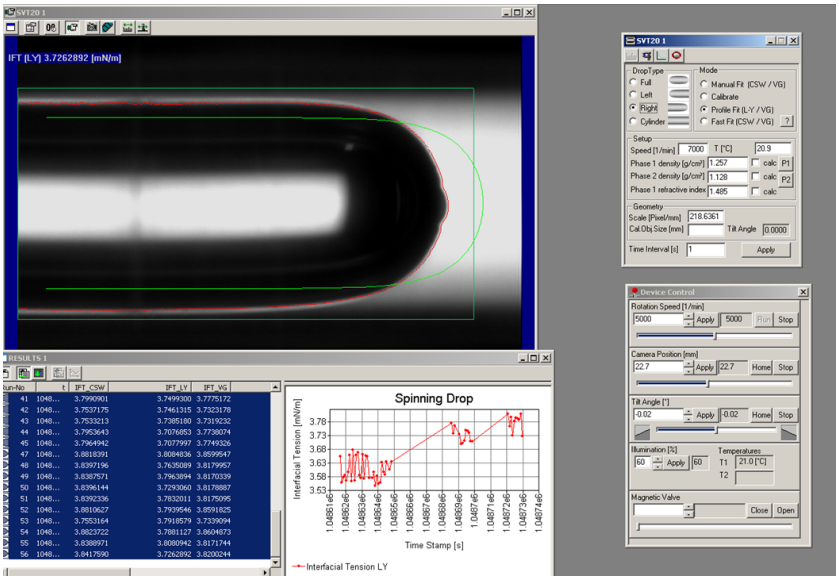

FIGURE 3.2: Screen shot showing the elongated oil droplet in the spinning drop tensiometer, as well as the fitting software.

The deformation stops when the interfacial tension and centrifugal forces balance. The radius of the drop perpendicular to the axis of rotation is a function of the angular frequency, density difference and the interfacial tension (Vonnegut, 1942). All of the former are known and with the help of software the dimensions of the drop are measured and the IFT calculated using the Young-Laplace method. The calculation is repeated 60 times and an average IFT is determined.

3.2 Core Flooding Experiments

3.2.1 Equipment

Core Flood Setup

The main objective of the setup is to reproduce oil bank build-up through surfactant polymer injection. The set-up is composed of a peek (Polyetheretherketone) core holder of varying length depending on the core it is housing. Two pumps (Blue-Shadow 40P) are used to inject the fluids into the system. The pumps can deliver a wide range of flow rates with minimal pressure pulses.

From an analysis point of view the most important aspects are accurate data in regards to mass balance and pressure. To achieve this two mass flow meters (mini CORI-FLOW^{TM}) are placed at the inlet and the outlet of the core holder to allow for an accurate mass balance calculation. The mass flow meters operate based on the Coriolis principle and therefore measure mass flow and density. The operating range of 5-200 g/h covers all flow rates that will be used during the core flood. Density is measured at an accuracy of 5 g/l. To get confirmation of when the injected fluids have entered and left the system a conductivity meter (AZURA CM 2.1S) was placed on both sides of the core. Since each fluid has a distinct conductivity response, the separate processes can be easily identified.

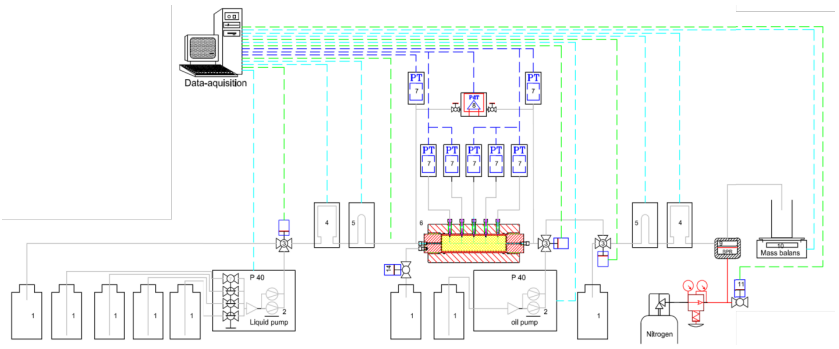

FIGURE 3.3: Schematic of the core flood set-up.

Pressure data is gathered by pressure transducers along the core as well as a delta pressure meter across the entire length. The primary source of data comes from the delta pressure meter which has an accuracy of 1% of its maximum range. An overview of the set-up can be seen in figures 3.3 and 3.4. All data is fed through a data processing program (LabView) which stores it as a text file.

To attempt to mimic some reservoir conditions a back pressure regulator was fitted to the system. During experiments this was set at 4 bar to simulate fluid pressurisation. The pumps also performed better with the back pressure when set to low flow rates. The entire set-up is placed in an oven to allow the experiments to be carried out at 30°C.

Fontainebleau Cores

The cores chosen for the experiments are drilled from Fontainebleau sandstone. The formation is known for its exceptional homogeneity. Its mineral composition is almost purely quartz (making up 99.5%) and a consistent grain size ranging between 100-300μm. These properties make it an ideal choice for core flooding experiments. Two different samples of Fontainebleau were used, one much more consolidated with lower porosity and permeability values. This difference is most likely caused by secondary cementation through quartz overgrowth (Saadi, 2017).

Various analyses of the rock samples showed porosity ranging from 6-11% and permeability starting at 10mD for the low permeability samples, up to 80mD for the high permeability cores. The properties vary vertically in the sequence. The wettability of the rock is water-wet meaning that the oil prefers to occupy the centre of the pores.

CT Scanner

To visualise the oil bank formation a number of experiments were performed under a CT scanner. The scanner used is a Siemens SOMATOM Definition. This is a medical grade scanner with dual-beam capabilities, one with an energy of 80kV and one of 140kV. Using both beams reduces artefacts and results in very clear images keeping in mind that the core holder and core are significantly more dense than what the scanner was designed for. The scans are made continuously as the core is pulled through the beams. The software then reconstructs the individual images in post-processing and a 3D composition is made.

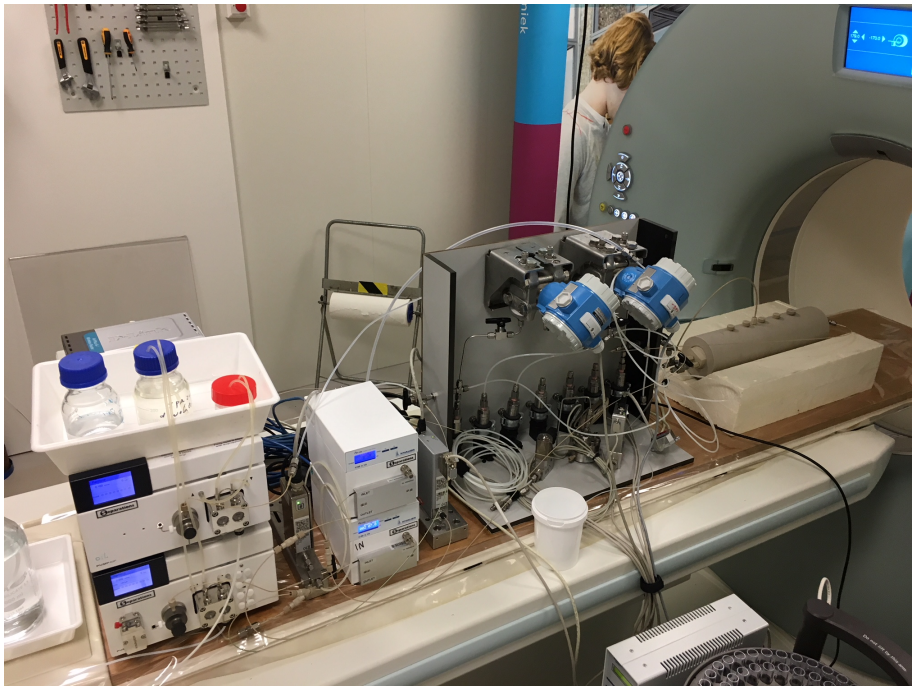

FIGURE 3.4: Overview of the set-up when placed in the CT scanner. Pumps are located on the far left, moving to the right the conductivity meters are flanked by Coriolis meters. Next is the pressure box containing the delta P and pressure transducers. Finally the core can be seen lying in the opening of the CT scanner.

3.2.2 Methodology

The core flooding procedure follows the method stipulated by (Al Saadi, 2016).

1. With the dry core in place the system is flooded with helium and checked for leaks.
2. The pressure is gradually built up and the helium is replaced by carbon dioxide since this is miscible with brine. A vacuum pump is then used to vacate the system.
3. Brine is slowly introduced and allowed to saturate the core and flow lines.
4. Once multiple pore volumes (PV) have been injected, brine permeability measurements can be carried out at various flow rates.
5. Tracer analysis for intial caluculation of pore volume and porosity. Brine flush after completion
6. Injection of oil via the outlet. Low flow rate ensures sufficient oil saturation and distribution around the core. A porous plate at the inlet allows brine to be displaced from the core and results in a spike in pressure once oil reaches the other end of the core.
7. *Water flooding*: One pore volume of brine is injected at the field rate, followed by multiple PV's at higher rates to produce as much oil as possible.
8. Second tracer run followed by brine flush
9. *Chemical flood*: Injection of 0.5PV of surfactant polymer at field rate. This is chased by 1PV of polymer.
10. Third tracer run
11. Core cleaning is done by flushing multiple pore volumes of brine followed by several PV's of isopropanol (IPA).

3.2.3 Tracer Analysis

One of the primary objectives of the research is for the results to be reproducible. Due to the limited number of cores multiple experiments will be done on the same cores. One of the conditions for reproducibility is that the initial conditions are not changing between runs. It was chosen to clean the core with isopropanol since this will remove any surfactant from the system and hopefully return the rock properties to their initial state. One disadvantage of using this is that it dehydrates the polymer solution causing precipitation of the polymer in the pore network. This polymer retention in the core will most likely occur in the smallest pore throats and restrict flow through it. By using a tracer analysis the accessible pore volume can be monitored at the different stages of the experiment.

For the tracer analysis a potassium iodide tracer is used at a concentration of 1%. The solution is injected at a rate of 0.01 ml/min. At the same time a fraction collector is used to collect the effluent at an interval of one test tube every 30 minutes. The system is left to run until one pore volume has been injected. The collected fractions are then analysed using a spectrometer to measure the concentration of potassium iodide against the injected pore volume.

Using the convection dispersion model the analytical solution is plotted through the data points from the fractional collector. Porosity and accessible pore volume can be determined by varying the coefficients to match the model to the data points.

Chapter 4

Phase Behaviour Analysis

The following chapter describes the results and observations of the phase behaviour tests conducted prior to the core flood experiments. The success criteria is determining the salinity at which the oil-surfactant system behaves optimally; defined by the presence of a third phase and when this microemulsion exhibits an interfacial tension in the ultra-low region.

4.1 Phase Behaviour

The behaviour of each test tube was captured by photograph for comparison. For each of the systems the overview of the optimal salinity is listed below:

TABLE 4.1: Optimum Salinity

System	SBA Conc. (wt%)	Optimum Salinty (wt%)
n-Dodecane	2	3.8
n-Dodecane	4	3.5
1-Iodododecane	2	4.5
1-Iodododecane	4	

Dodecane

For the dodecane system a Winsor type I behaviour is seen up until a salinity of approximately 3wt%. From this point on the system exhibits a third phase microemulsion up until 4.5wt%, where it transitions to Winsor Type II. Looking at the more focused scan using increments of a quarter percent, the system initially shows a larger volume fraction of brine in the microemulsion. Based on the observed solubisation parameters the optimum was chosen at 3.75wt%.

An interesting observation for the dodecane systems is that the optimum salinity seems to vary over time. After initial equilibration the lower salinity micro emulsions seem to disperse through the oil phase while the higher salinities seemed to remain stable. Some controversy still exists with regards to how much time the samples should be given to equilibrate. To ensure consistency the IFT tests were done approximately two weeks after preparing the tubes.

Iodododecane

The iodododecane system exhibits similar behaviour however due to the density of the oil it now sits below the brine. The three-phase region occurs at a higher salinity as the dodecane, starting at 3.5% and extending all the way beyond 6%. Optimum was recorded as 4.5%, these results can be found in Appendix A.

FIGURE 4.1: Phase behaviour of the dodecane-oil system using 1% O242 surfactant and 4% SBA as co-solvent. Salinties of the tubes are 2,3,3.25,3.5,3.75,4,5, respectively.

Co-Solvent Concentration

Comparing the two and four percent co-solvent systems, the volume of micro emulsions is greater if less co-solvent is present. The interface is also less defined and more translucent. This is because as the concentration of co-solvent increases the oil-water interface becomes more flexible and the dispersed droplets can become smaller. Increasing the concentration of SBA also reduces the optimal salinity, due to the hydrophobicity of the co-solvent. Eventually the higher co-solvent concentration was chosen. Although this negatively impacts the microemulsion volume the viscous phase is not formed and equilibration time is greatly reduced.

4.2 IFT Measurements

The results from the spinning drop tensiometer are given in the graph below. IFT is plotted as a function of salinity on a log scale, giving the characteristic "V" shape culminating at the optimum. For the lower salinities the lack of sufficient microemulsion volume meant that the measurement could not be properly done. It can be assumed that these values will be equal to, or greater than the initial value of interfacial tension. For these results it is assumed that the surfactant is fully contained by the water phase and oil-water IFT tests show marginal differences when compared to a test system without surfactant. When micro emulsions are present however the IFT values drop into the ultra-low region.

Optimum

The optimum for dodecane from the IFT measurements is **3.75%** which coincides with the result from the phase behaviour test. Iodododecane exhibits an optimum at **4.5%** which is slightly lower than what was chosen for the phase behaviour. Due to the qualitative nature of the phase behaviour measurements it was chosen to use the value from the IFT test.

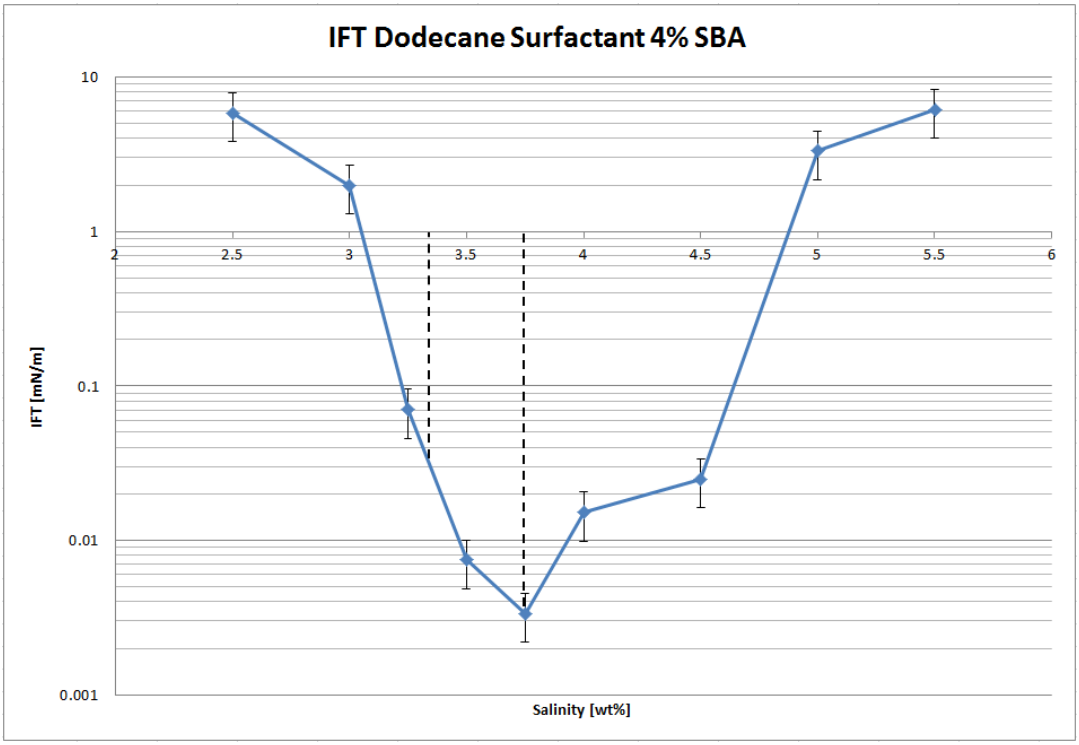

FIGURE 4.2: Interfacial tension data from the spinning drop tensiometer. The optimum and underoptimum salinities are marked.

Underoptimum

For both oils a value for underoptimum phase behaviour was also chosen. As mentioned, there are certain advantages to injecting the surfactant at underoptimum salinity. With the IFT data a salinity can be chosen where these advantages are realised, but the IFT is still sufficiently low. For dodecane underoptimum was chosen at 3.25% and 4% for iodododecane.

Chapter 5

Results: Core Flood

In this chapter the core flood experiments are discussed. An overview of the core properties and saturation data are given in table 5.16 at the end of the chapter. The first data set will be discussed in detail followed by the relevant results from the other experiments.To get an idea of the displacement processes occurring in the core floods the CT results will be discussed first.

5.1 17cm Low Permeability

5.1.1 CT Scan

Oil Saturation & Waterflood

The first experiments done under CT were the 17cm low permeability cores. Throughout the different stages of the experiment scans were taken to visualise the process and ensure everything was going to plan. The following series shows the oil saturation stage with the oil being injected through the outflow (right side). Over time the front advances along the core displacing the brine. The iodide bonded to the dodecane chain results in strong attenuation of the x-rays causing a very distinct contrast between the oil and water phases.

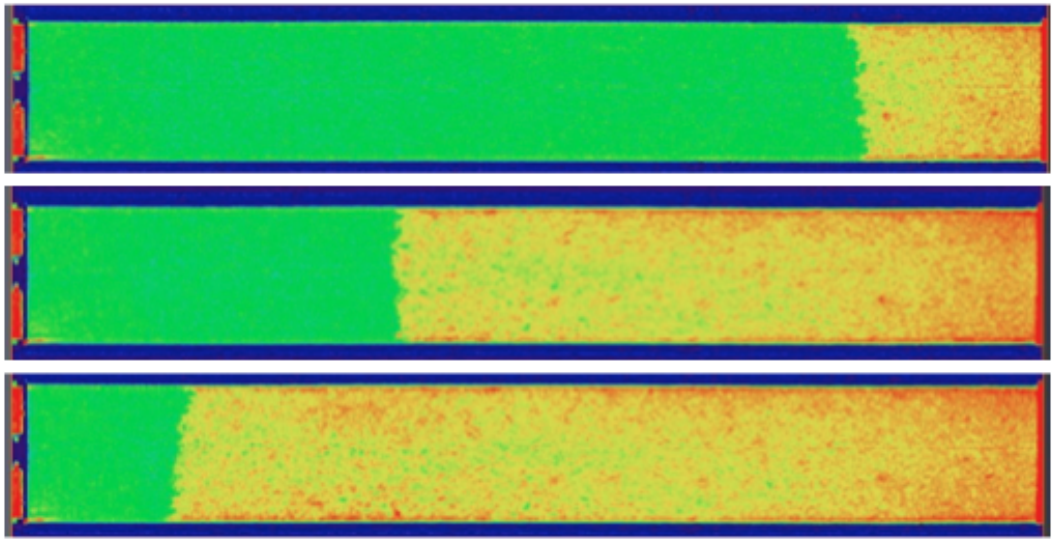

FIGURE 5.1: CT scans showing iododododecane injected (from right) into a core saturated with brine. The iodide attenuates the x-ray signals resulting in the bright (red) signature.

Surprisingly, the scans were even able to show the waterflooding stage of the process. In other experiments the strong response of the iodododecane drowned out the weaker signal of the brine. Coupled with a low waterflood recovery factor meant that this stage was not always visible on the CT scans. Additionally the scans show the porous plate (left side) which aids in the oil filling process.

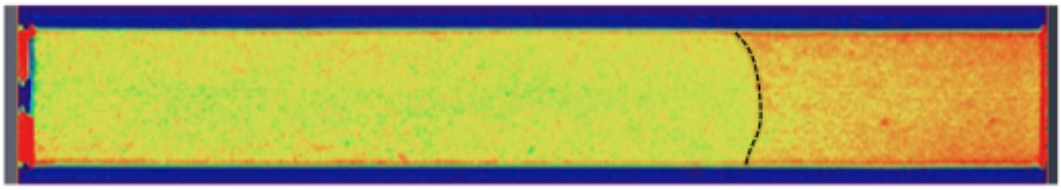

FIGURE 5.2: CT scan showing the waterflooding of the 17cm core. The brine is advancing from the left, displacing the oil.

Surfactant Polymer

The surfactant polymer injection was the focal point of the CT scan images. Scans were taken at intervals of roughly 0.2 PV to monitor oil saturation and oil bank formation. For the 17cm cores The initial image was promising. As the slug enters the core the decrease in x-ray attenuation indicates that the waterflood residual-oil is being mobilised. The Houndsfield units show a significant increase in oil saturation just in front of the advancing surfactant polymer slug. This area is indicated in figure 5.3 and could be the beginning of an oil bank.

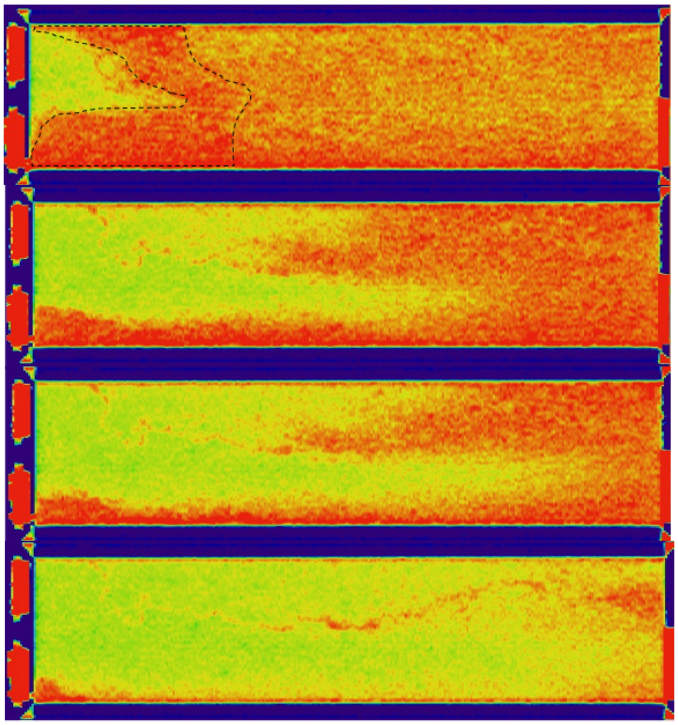

FIGURE 5.3: CT scan showing the chemical flood of the 17cm core. The beginnings of an oil bank can be seen which dissipates due to an inhomogeneity.

Unfortunately as the flood continues it is clear that there is a pronounced inhomogeneity in the core. The slug splits between two layers and exhibits preferential flow through the bottom layer. This stops the stable displacement and any further oil bank formation.

5.1.2 Production Data

The second source of information is the inflow and outflow data from the sensors in the set-up. For most experiments this is the only piece of information available, for these 17cm and the 30cm high permeability cores it was possible to link the production and CT data together. Initial oil and water saturations were determined by material balance. The data was processed to determine flow rate from mass flow rate and density, and oil production by comparing the density of the injected liquid to the density of the produced fluids. All of the data is plotted against the dimensionless parameter pore volume which allows comparison between the experiments. The following graph 5.4 shows the data in graphical format:

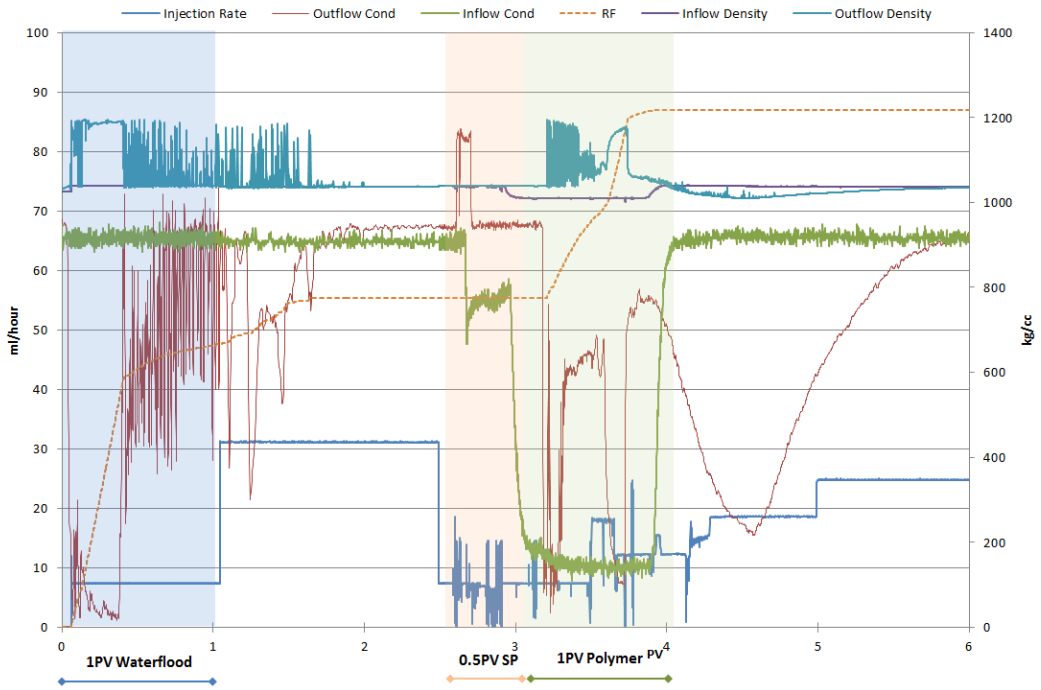

FIGURE 5.4: Production data from the 3rd experiment of the 17cm low permeability core flood performed in the CT scanner.

A transparent overlay has been added for clarity. The injection is plotted in blue and is always set to 6ml/hour which is equal to the field rate of 1 ft/day. After each stage the injection rate is increased to produce any remaining oil and to vacate the core of any polymer. Spikes in the injection rate during the chemical flood are due to issues with the pump. Polymer particles would either interfere with the pump head or clog the inflow lines, this was solved by manually clearing the pump head which lead to spikes in flow rate that were picked up by the Coriolis meter.

Waterflood

The initial pore volume (blue) represents the **waterflood** portion of the experiment. The first indication of oil production is the sudden spike in outflow density, which coincides with the density of iododododecane (1180kg/cc). The conductivity also drops and then slowly increases after water breakthrough (0.3PV). After this slug flow dominates which is shown by the fluctuations in density and conductivity. Unfortunately the conductivity meter has an exaggerated response to sharp changes which causes the behaviour seen in some experiments. Recovery factor from the water flood is high (53%) which explains why the water flooding was picked up by the CT scan.

Chemical Flood

Upon injection of the surfactant polymer slug a slight decrease in conductivity is seen, this is the surfactant polymer. After 0.5PV the conductivity drops even further as the polymer slug enters the system. Its salinity was chosen to be approximately 1wt%. As a result the system transitions to under-optimum as the flood proceeds which could result in the produced surfactant entering the brine phase and less oil in the microemulsions. After 0.6PV of chemical flooding the first oil is produced. As seen on the CT scan the inhomogeneity means that an oil bank was not formed and therefore production shows alternating slugs of oil and surfactant coming from the bottom layer. The two-step response in the recovery factor confirms the presence of two layers seen in 5.3. The second layer seems to produce a small bank of oil at around 3.6PV in the graph. The monotonous increase in density and drop in conductivity show that 15% of the oil from the chemical flood was as clean oil.

Pressure Response

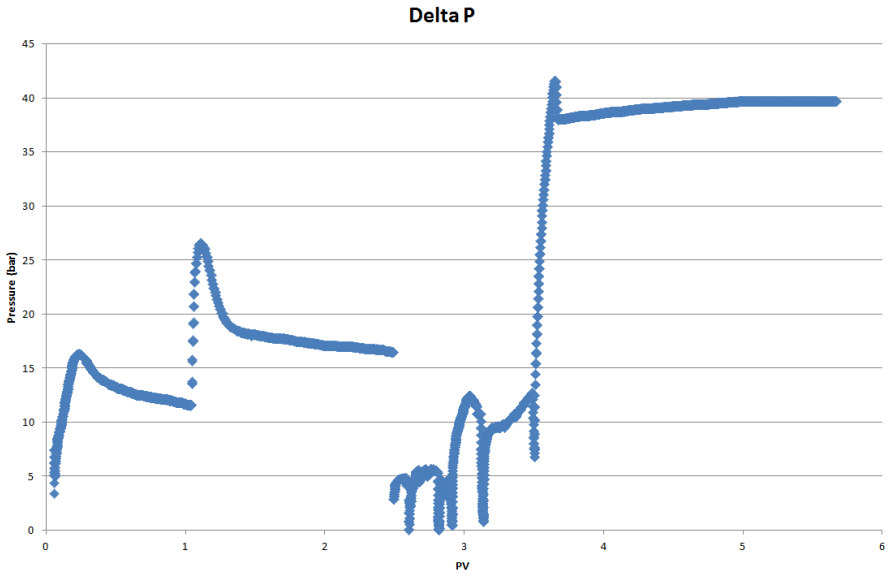

FIGURE 5.5: Pressure data from the 3rd experiment of the 17cm low permeability core performed in the CT scanner.

Pressure data is needed later on for the relative permeability analysis, but it also gives an indication of the mobility control during the experiment. Looking at the pressure difference across the core the build up during the water flood can be seen up until water break through. The surfactant slug does not seem to come across which may be due to the issues mentioned before. It is not until the arrival of the polymer slug that the increasing pressure gradient indicates favourable mobility of the front. This could explain why the oil bank is only seen later on when the more viscous polymer is less affected by the inhomogeneity. A larger surfactant polymer slug could have overcome this problem.

5.1.3 Non-CT Production Data

Three more experiments were done using the 17cm low permeability cores. The experiments showed a high degree of reproducibility. Oil recovery from the water flood was 35-40% with the chemical flood producing another ~40%, giving an ultimate recovery in the range of 80-85%. In two of the experiments an oil bank was formed successfully with oil breakthrough occurring at 0.7PV after start of chemical injection. Of the oil produced during the chemical flood approximately 23% was clean oil from the oil bank. The remaining oil was produced as microemulsions.

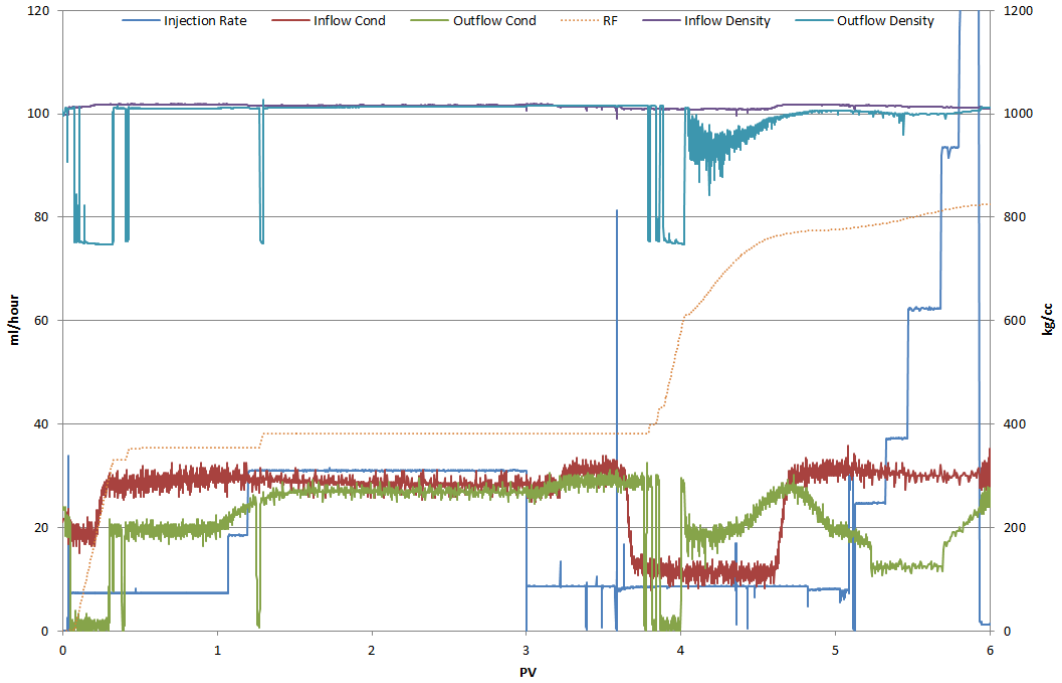

FIGURE 5.6: Production data from the 3rd 17cm experiment done outside of the CT.

Two of the chemical floods were unsuccessful at forming an oil bank. Later it was discovered that this was caused by improper storage of the surfactant solution. Left in a glass beaker under a parafilm the co-solvent most likely evaporated out of the solution. As mentioned in chapter 3, decreasing co-solvent concentration will alter the optimum salinity. These experiments were unknowingly done at overoptimum conditions and therefore the surfactant was ineffective.

5.2 39cm Low Permeability

For the next experiments the core length was increased to 39cm with the objective of seeing how core length influences oil bank formation.

5.2.1 CT Scan

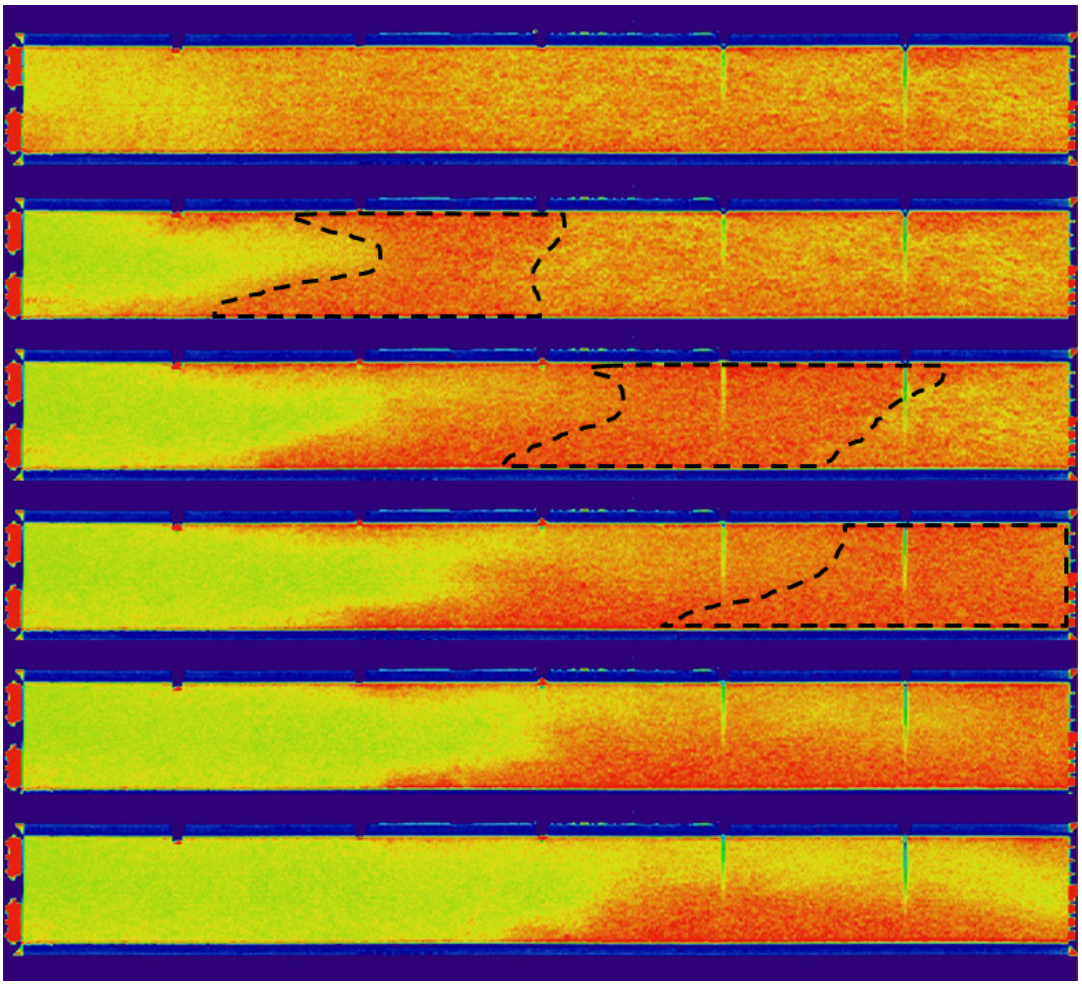

FIGURE 5.7: CT scans taken at 0.2 PV intervals showing surfactant polymer propagation and oil bank formation.

From the scans we see the surfactant "tongue" forming as more SP is injected. This is an indication that the displacement is not stable. In this experiment and the following one the same increase in oil saturation as in the 17cm core is seen preceding the surfactant front. However instead of dissipating due to an inhomogeneity the front is now able to build and propagate through the core. This is visual confirmation that a oil bank has been created by surfactant polymer injection. Towards the end some degree of gravity override can be seen, keeping in mind that the oil is the denser phase in this experiment.

5.2.2 Production Data

Looking at the production data of the CT experiment, the waterflood recovery factor is relatively low at 28%. This is a possible reason why the chemical flood was very effective. The chemical flood data shows a relatively clean oil bank compared to other Iodododecane experiments, however the characteristic slug flow is also present. The oil bank begins to be produced 0.35PV after SP injection and approximately 30% of the oil initially in place is produced in the oil bank. After this the gradual rise in conductivity indicates microemulsion breakthrough. This coincides with the gravity override seen on the CT scan which explains why we see almost 0.8PV of microemulsion production.

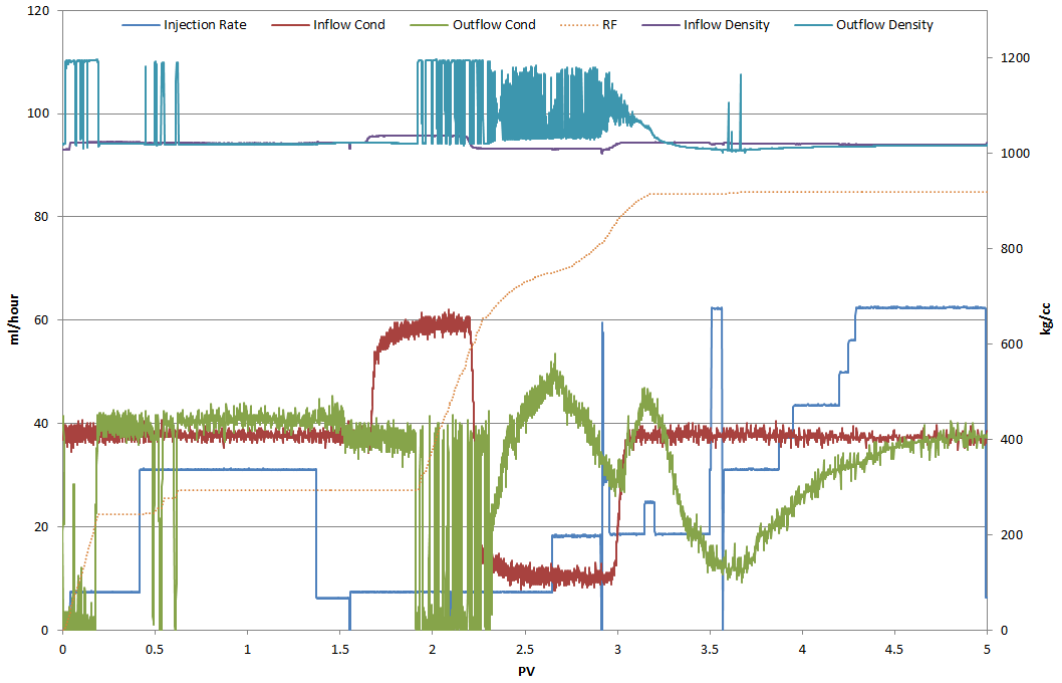

FIGURE 5.8: Production data from the 2nd 39cm experiment done under the CT Scan.

Total recovery factor after chemical flood is approximately 85% with the last 15% produced in microemulsions.

5.2.3 Non-CT Production Data

Two experiments were done with dodecane and showed reproducible results. The average recovery from the water flood was 30% leaving a residual oil saturation of 0.55 after waterflood. The low waterflood recovery is due to the lower initial oil saturation. The injection data shows that we were only able to achieve an oil saturation of 0.7 which is significantly lower compared to other experiments. The surfactant polymer flooding recovered 28% as clean oil starting 0.3PV after chemical injection. The microemulsion tail contained another 20% of incremental oil production resulting in a cumulative recovery of 81%. It is possible to characterise another type of oil bank in these experiments. Initially slug flow is observed with an increasing fraction of oil over time, 0.25PV later the oil production becomes continuous which is the oil bank.

5.3 7cm High Permeability

The following experiments used cores with similar mineralogical composition but different rock properties. The sandstone was much less consolidated with porosities ranging from 10-14% and permeabilities between 60 to 80mD.

5.3.1 Production Data

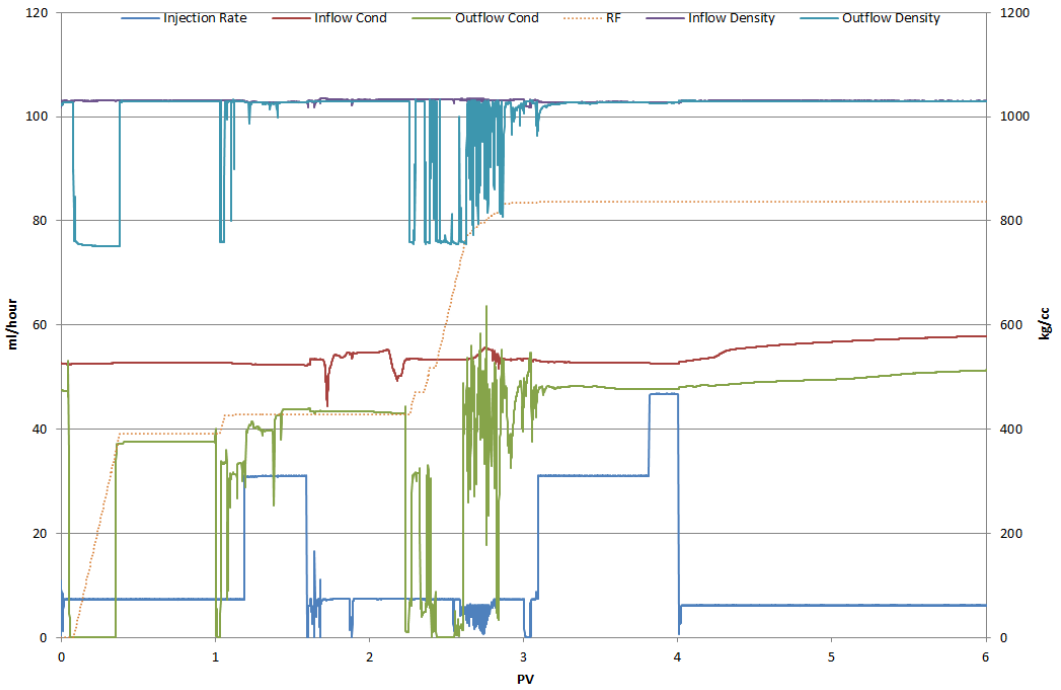

FIGURE 5.9: Production data from the 7cm high permeability core-flood experiment.

The water flood in the 7cm core recovered 40% of the dodecane. The total recovery after the chemical flood equalled 85% with the majority coming from oil bank production. The microemulsion tail only produced 5% of the incremental oil. The shorter core length reduces the degree of dispersion and effects of any heterogeneities. One important observation is the malfunction of the inflow conductivity

meter. It reads an almost constant value throughout the experiment whereas other experiments showed distinct changes in conductivity for the surfactant polymer and the polymer. Given as the polymer was made as a large batch for multiple experiments the meter itself is most likely responsible for the erroneous readings.

5.4 17cm High Permeability

5.4.1 Production Data

Four experiments were done using the 17cm cores of the high permeability variant. The first three experiments produced almost identical results. For these experiments the waterflood recovery was 40% and the ultimate recovery after the surfactant polymer was around 80-85% in every experiment. From the production data an oil bank seems to form in all of the experiments, which becomes visible 0.4PV after the start of SP injection. Almost 35% of the oil is clean oil with only 5-10% was oil-in-microemulsion. This points to the low-salinity polymer transitioning the system to Winsor type I phase behaviour over the course of the flood.

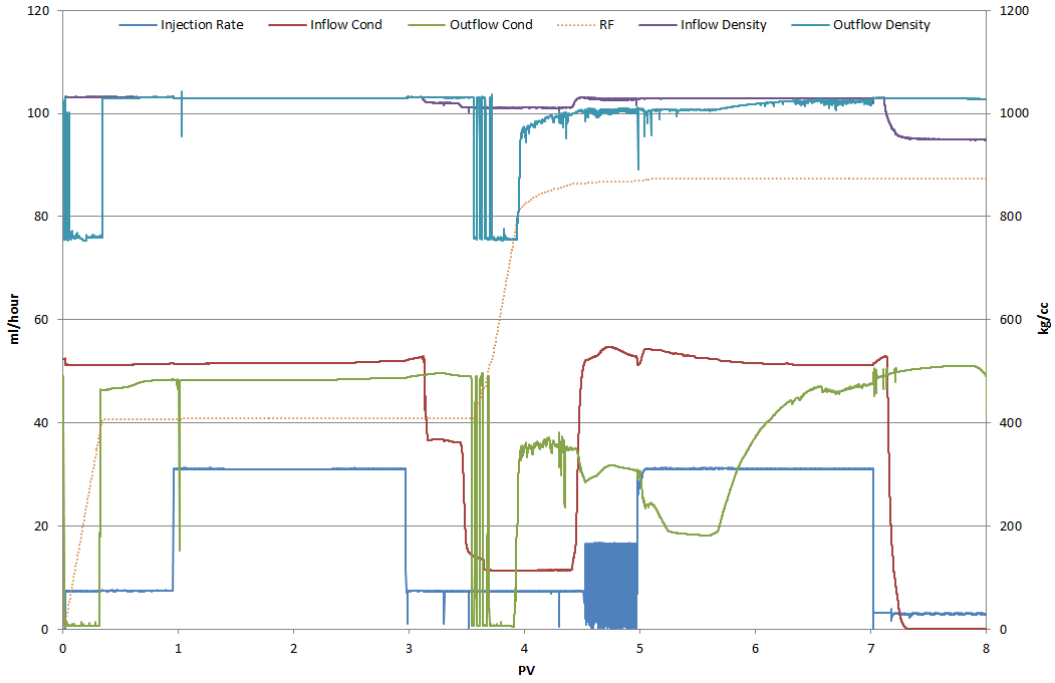

FIGURE 5.10: Production data from the 17cm high permeability core-flood experiment.

The last experiment produced different results. Waterflood recovery was significantly lower at 25% which is half as effective as in the rest of the series. Oil saturation after waterflood was 0.52 compared to the usual 0.4-0.45. With this higher oil saturation the oil bank seems to be more developed with more clean oil produced and only a small fraction produced in microemulsion.

5.5 30cm High Permeability

The final set of experiments were done on 30cm cores both in and outside of the CT scanner.

5.5.1 CT Results

From the scan following the waterflood its clear that there is preferential flow through a part of the core. The area outlined below shows a lower residual oil saturation after waterflood than the rest of the core. A large pocket of oil is left on the upper side of the core.

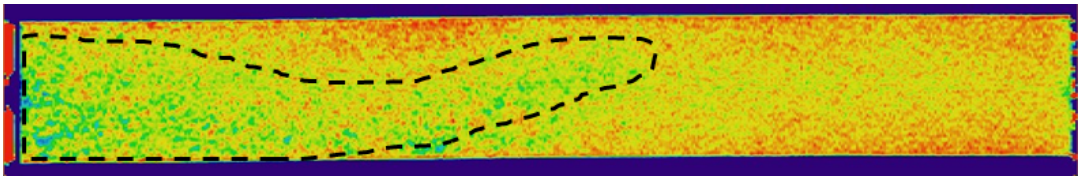

FIGURE 5.11: Scan showing area of lower residual oil due to fingering effects.

Based on previous experiments with iododecane, the surfactant polymer will most likely follow the same path as shown above; leading to the multiphase slug flow without successful oil bank formation.

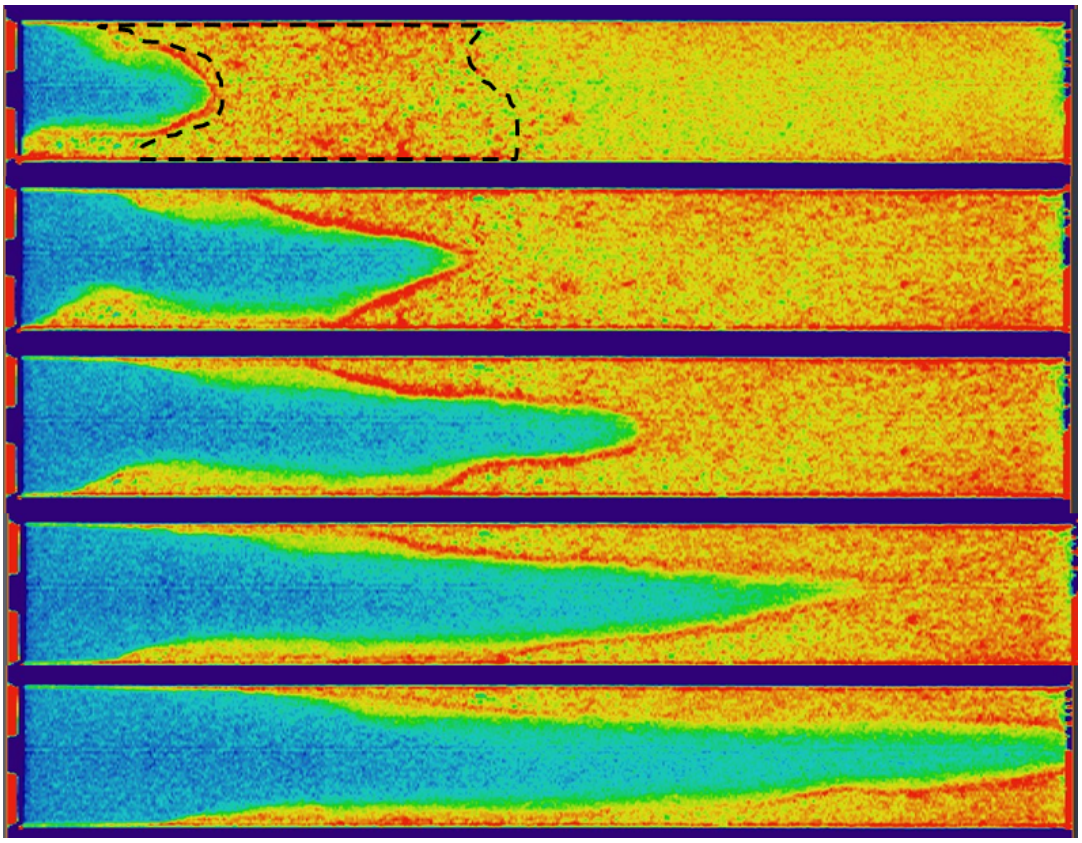

FIGURE 5.12: Scan showing Surfactant Polymer flood of 30cm high permeability core in intervals of 0.15PV.

Up until about 0.4PV of injection the slug seems to be sweeping relatively well. The start of oil bank formation can even be seen (marked in Fig. 5.11). However when it reaches the area highlighted before the front breaks down and exhibits poor stability up until SP breakthrough after approximately 0.8PV of chemical injection. After approximately 1.6PV the polymer is able to sweep the remaining sections of the core and oil production concludes.

CT Production Data

From the production data (Fig. 5.13) the waterflood recovery factor seems to be in line with other experiments however it is possible that the majority of the residual oil is in the upper section of the core as seen in the scan. This would skew the recovery factor downwards even though average residual oil saturation is lower.

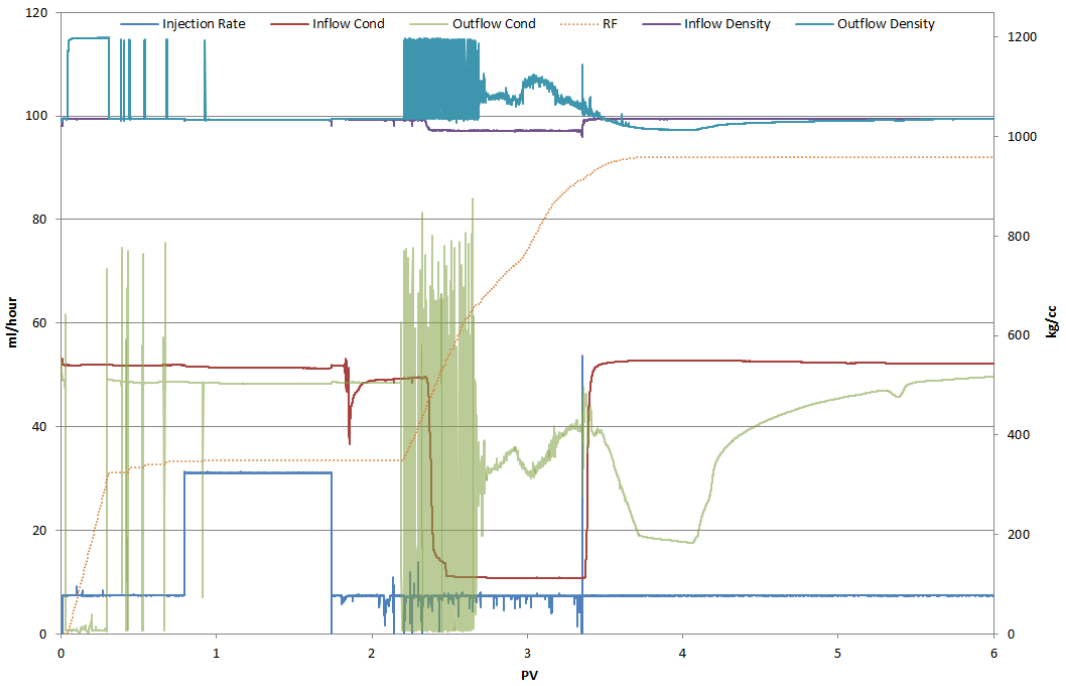

FIGURE 5.13: Production date of the second experiment of the 30cm high permeability core done under the CT scanner.

The production data confirms a number of other observations made from the CT images. We see slug flow starting 0.3PV after the start of SP injection and continuing for 0.6PV which is when SP breakthrough is seen. What is unique about these experiments is a period of decreasing oil cut right after the end of slug flow. Oil production slows down and then increases again ending with a microemulsion tail seen in other data. It is possible that the surfactant causes an unstable interface with the iodododecane. The SP slug is produced first followed by an increase in oil production as the polymer front displaces more oil due to better mobility.

5.5.2 Production data

A single experiment was done outside of the CT room which supports the observations mentioned above. Waterflood recovery in this experiment is higher and the production seems to point to a more stable, piston-like displacement. The initial oil

bank contains approximately 80% of the oil production from the chemical flood with the remainder produced as microemulsions. Total recovery for this experiment was 90% Which is the highest of all the experiments.

5.6 Discussion

5.6.1 Reproducibility

For every set of core floods the results were deemed reproducible if: the recovery factor differed by less than 5%, and the displacement behaviour was similar. For example step-wise production due to inhomogeneities should be seen across all data sets. Analysing the production data from of the experiments for reproducibility the exceptional results of the 17cm high permeability cores can be highlighted.

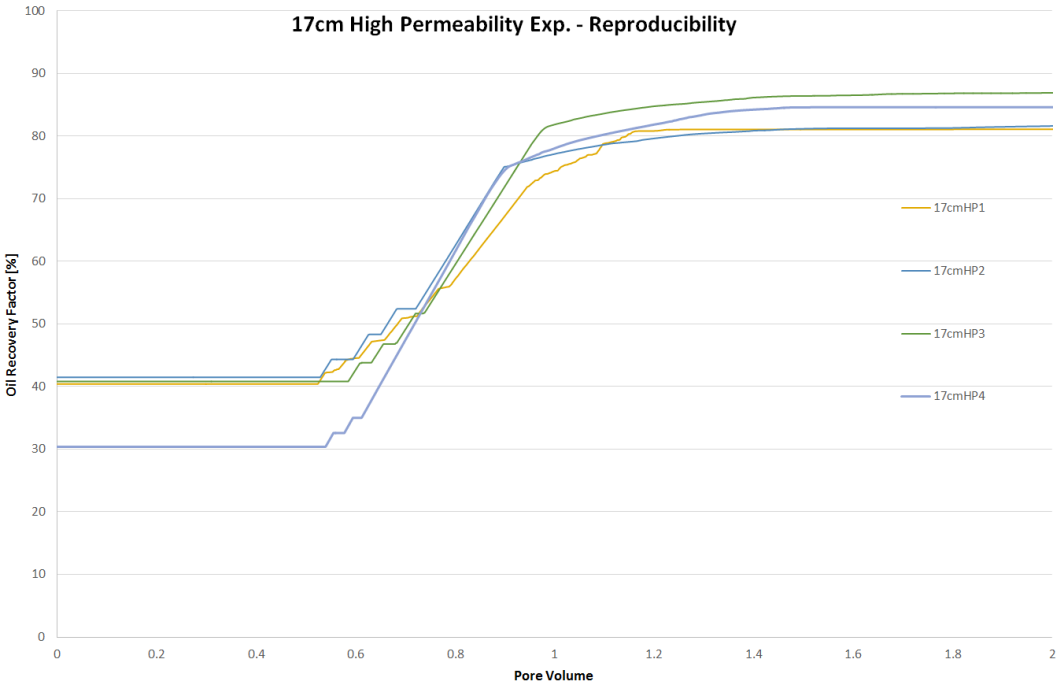

FIGURE 5.14: Recovery factor of the 17cm high permeability cores, showing excellent reproducibility between them.

Four separate experiments were done using this single core. The recovery factors fall within a range of 82-86% with a 4-step pattern seen at the start of the oil bank in every experiment. The last experiment had significantly lower water flood recovery however the production curve and ultimate recovery falls within the other experiments. This confirms that the surfactant polymer slug has increased the capillary number to similar levels as the other runs leaving the system at a comparable position on the capillary desaturation curve.

The other experiments were repeated until a similar degree of reproducibility was seen. The first run of each set often showed a slightly different response probably due to unconsolidated grains moving through the core. After this the core seems to reach a stable state and the floods become more similar. In Figure 5.14 this is seen in a slightly lower recovery rate. This effect is more prominent in the low permeability cores.

Although not all successful, the CT scans also allowed us to judge the reproducibility from a qualitative standpoint. Although the snapshots in Figure 5.15 are not taking at identical times the tongue formation and path through the core are similar in both cases. Three time steps are shown with two images (x- and y-direction) for each.

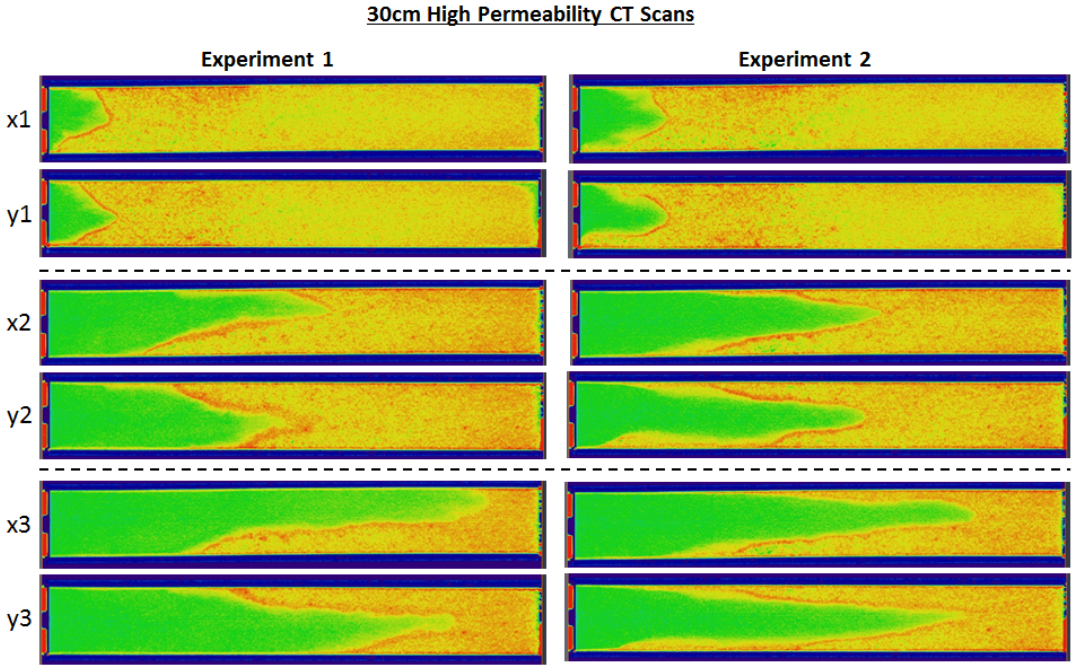

FIGURE 5.15: CT scans showing reproducible displacement patterns between the two experiments.

5.6.2 Decreased Surfactant Polymer Slug Size

In two of the experiment sets the injected SP slug size was decreased to 0.3PV rather than 0.5PV. This was done to test the sensitivity of the recovery factor on slug size, with obvious economical motives. Comparing the production data of the low permeability chemical floods a decrease in recovery factor of 10% is seen in both of the experiments with good reproducibility between them. Residual oil saturation after the chemical flood with the smaller slug size is 0.21 which is significantly more than in all other experiments, regardless of length. Little to no difference is seen in the oil bank behaviour or in the recovery factor in the high permeability cores. A decrease in slug size will reduce the ratio of active surfactant to pore volume and the sweep efficiency of the flood. Most likely the homogeneity of the core is good enough to ensure sufficient SP sweep even with a smaller slug size.

5.6.3 Underoptimum Injection Conditions

Only one experiment was carried out at underoptimum conditions so the reliability of the data and any conclusions can be disputed. Initial observations show that a larger fraction of the oil from the chemical flood is produced in the oil bank with less oil-in-microemulsion. Overall production was lower for this experiment. Purely from a recovery standpoint this approach seems less effective however it does not take into account the added benefits of the salinity buffer for the divalent electrons.

Core Length (cm)		7						17								30		39	
Flood#		V1	V2	CT2	CT3	V1	V2	V3	V4	V5	V1	V2	V3	V4	V1	V2	V1	V2
Rock Type		HP Fontainebleau				LP Fontainebleau						HP Fontainebleau			HP Fontainebleau		LP Fontainebleau	
PV (ml)		14.5				17						23			30		33	
Porosity (%)		11.2				9.8						11.2			11.2		9.8	
Brine Permeability (mD)		80				1.4						70			65		1-2	
Oil Injected (ml)		11.0	10.2	12.6	12.8	13.0	12.6	12.2	12.8	12.7	18.0	17.6	17.2	15.5	26.0	25.0	23.0	23.0
WF	Soi	0.76	0.70	0.74	0.75	0.76	0.74	0.72	0.75	0.75	0.78	0.77	0.75	0.67	0.87	0.83	0.70	0.70
	Sor	0.46	0.43	0.30	0.22	0.45	0.42	0.42	0.43	0.43	0.47	0.44	0.44	0.47	0.58	0.54	0.53	0.49
Chemical	Soi	0.46	0.44	0.30	0.22	0.45	0.42	0.42	0.46	0.43	0.47	0.44	0.44	0.47	0.58	0.54	0.53	0.49
	Sor	0.12	0.12	0.06	0.08	0.11	0.08	0.10	0.20	0.20	0.15	0.13	0.09	0.10	0.10	0.19	0.07	0.13
									Surfactant Polymer Slug									
SP Slug Size (PV)		0.5	0.5	0.5	0.5	0.5	0.5	0.5	0.3	0.3	0.5	0.5	0.3	0.3	0.5	0.5	0.5	0.5
C_{surf} (% active)										1% Enordet O242								
$C_{co\text{-}solvent}$ (wt%)										4% 2-Butanol								
$C_{polymer}$ (ppm)		500	500	550	550	500	500	500	500	500	500	500	500	500	500	500	500	500
μ_{slug} (cp)		8.7 @6s^{-1}	8.7 @6s^{-1}	12.2 @6s^{-1}	12.2 @6s^{-1}	10.1 @6s^{-1}	10.1 @6s^{-1}	10.1 @6s^{-1}	10.1 @6s^{-1}	10.1 @6s^{-1}	11.0 @6s^{-1}	11.0 @6s^{-1}	11.0 @6s^{-1}	11.0 @6s^{-1}	10.0 @6s^{-1}	10.0 @6s^{-1}	10.0 @6s^{-1}	10.0 @6s^{-1}
Salinity (ppm)		38000	38000	45000	45000	38000	38000	38000	38000	38000	38000	38000	32000	32000	38000	38000	38000	38000
										Polymer Drive								
$C_{polymer}$ (ppm)		680	680	750	750	680	680	680	680	680	680	680	680	680	680	680	680	680
$\mu_{polymer}$		14.2 @6s^{-1}	14.2 @6s^{-1}	17.1 @6s^{-1}	17.1 @6s^{-1}	15.5 @6s^{-1}	15.5 @6s^{-1}	15.5 @6s^{-1}	15.5 @6s^{-1}	15.5 @6s^{-1}	15.5 @6s^{-1}	15.5 @6s^{-1}	15.5 @6s^{-1}	15.5 @6s^{-1}	15 @6s^{-1}	15 @6s^{-1}	15 @6s^{-1}	15 @6s^{-1}
Salinity (ppm)		10000	10000	10000	10000	10000	10000	10000	10000	10000	10000	10000	10000	10000	10000	10000	10000	10000
										Oil Recovery Results								
WF Recovery (%)		42.8	44.6	55.1	54.4	42.5	44.3	40.5	43.6	43.1	40.4	41.5	40.8	30.4	33.6	36.1	23.2	30.2
Ultimate Recovery (%)		83.7	84.2	88.8	96.9	89.7	88.2	82.7	72.5	72.0	81.2	81.8	85.4	84.9	90.2	86.2	89.7	85.4

FIGURE 5.16: Table showing an overview of results from the successful core flood experiments.

Chapter 6

Results: Analytical JBN Method

The following chapter presents the results of applying the analytical JBN method to the production data from Chapter 5. When processing the data attention was paid to the quality and accuracy of the pressure data. The model is sensitive to unexpected changes in pressure. For certain data sets the pressure response could be smoothed or interpolated, however in some cases the data could simply not be used. This was due to calibration issues, faulty pressure sensors, or equipment malfunction (blockages, backpressure fluctuations, etc.). An example of a faulty data set is given in Appendix D.

6.1 17cm Low Permeability

The production results are analysed using JBN and plotted below:

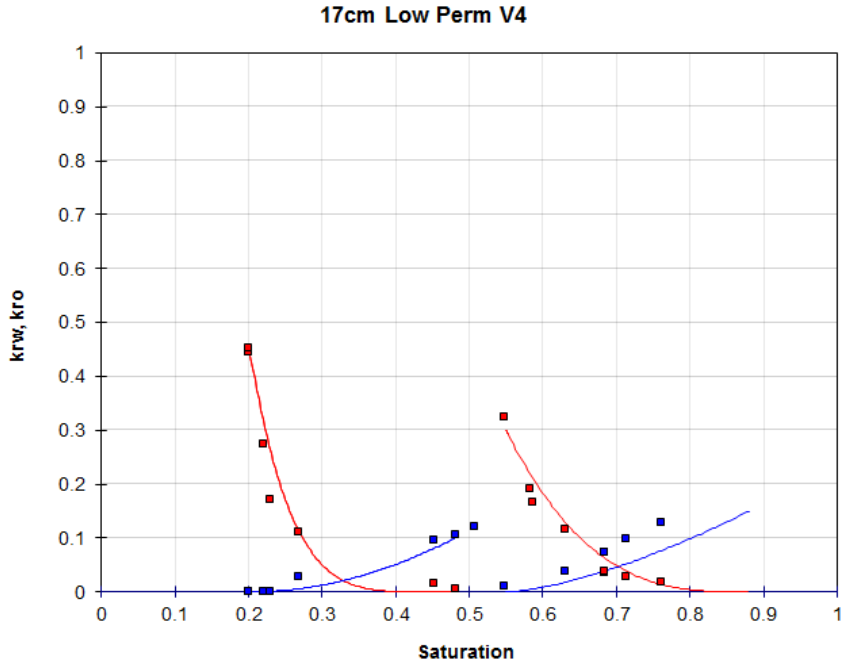

FIGURE 6.1: Relative permeability curves resulting from the JBN analysis of the 17cm production data.

The front of the waterflood in many experiments seems to be particularly sharp. This means that there are very few data points in the two-phase flow region which

are needed for calculating the intermediate relative permeabilities. This is why a "gap" can be seen in the water flood curves. Where possible the points were modelled using Corey relations if the fit was acceptable.

Calculating relative permeabilities of the 17cm chemical flood data did not require any modifications to the JBN method. The immediate onset of the oil bank followed by surfactant polymer breakthrough and a subsequent two-phase flow region leads to the curves on the right. Comparing the two we see a shift right due to the increase in S_{wi} from the waterflood and oil bank production. Residual oil saturation after the chemical flood is 0.12. Initial oil relative permeability is lower for the chemical flood however it decreases less per unit of S_w increase.

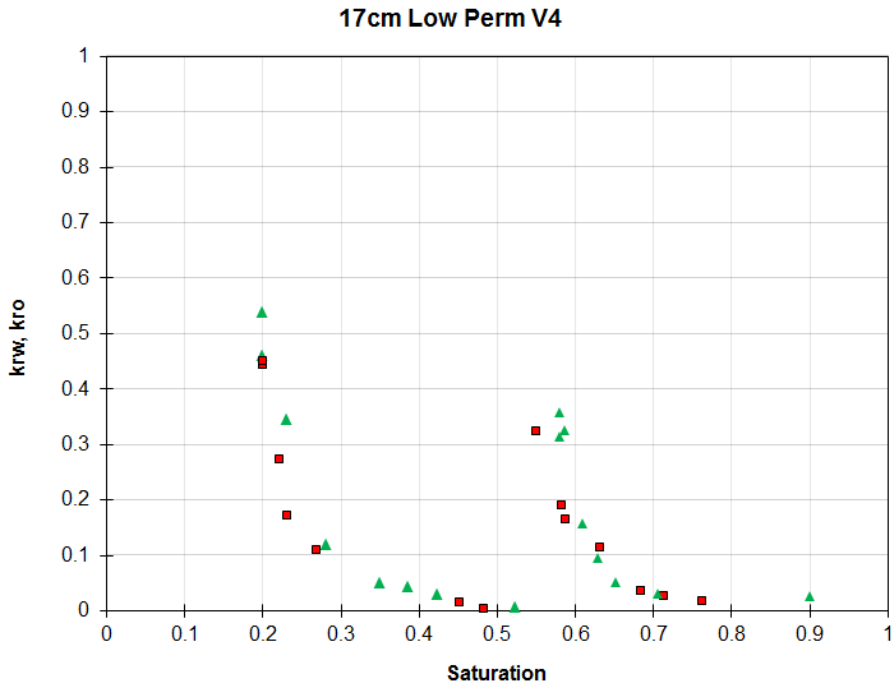

FIGURE 6.2: Oil relative permeability curves resulting from the JBN analysis of two different 17cm core floods.

The chart above plots two data sets on top of each other to examine the reproducibility of the JBN interpretation. Since one of the criteria for the production data is that the core floods must be reproducible it can be expected that similar inputs will lead to similar outputs. Indeed the rel-perms from the different runs are the same. Small discrepancies are most likely caused by the data points chosen and/or pressure variations.

6.2 39cm Low Permeability

The results for the 39cm cores reflects the higher residual water saturation observed in the core flood experiments.

When analysing the chemical flood data the method was slightly altered to account for two factors. First, the slug flow that precedes the oil bank will result in incorrect values for the subsequent data points. This is because the JBN method assumes piston like displacement with three stages: First single-phase flow of the displaced phase, secondly a region of two-phase flow after initial breakthrough of

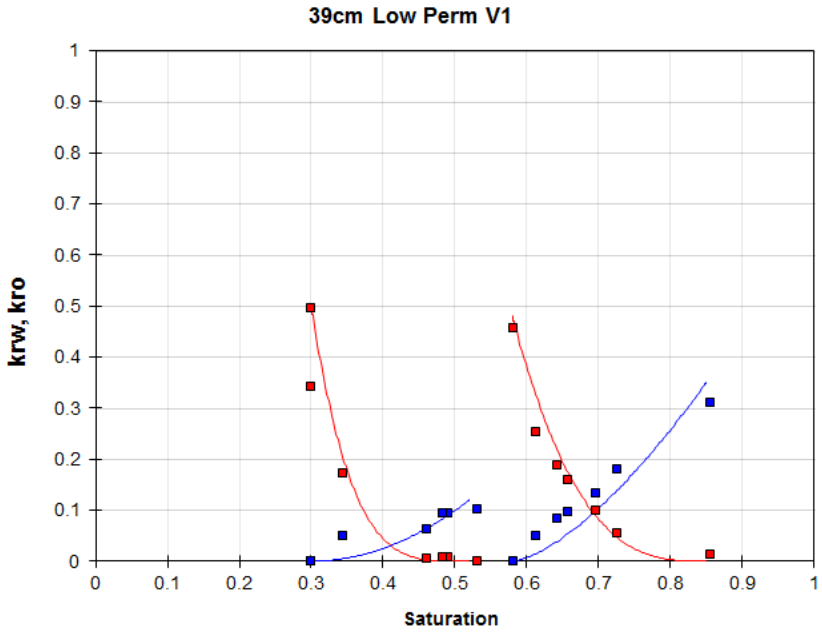

FIGURE 6.3: Relative permeability curves resulting from the JBN analysis of the 39cm production data.

the displacing phase, and finally a period of single phase flow of the displacing fluid. The pressure readings during the slug flow is so erratic that it is hard to trust the data after smoothing.

Secondly this initial oil production starts 0.2PV after the start of chemical injection. Given that 0.12PV is dead volume of the inflow, the slug has barely entered the core. At this point the majority of the matrix is still under waterflood relative permeability conditions. By shifting the starting point of the analysis to the start of the oil bank we are able to apply JBN as well as capture a more accurate representation of the chemical relative permeabilities.

6.3 7cm High Permeability

The 9cm relative permeability results are given next. Looking at the K_{ro} values we see a lower end point relative permeability at the start of the chemical flood. They also remain higher as the water saturation increases compared to the water flood data.

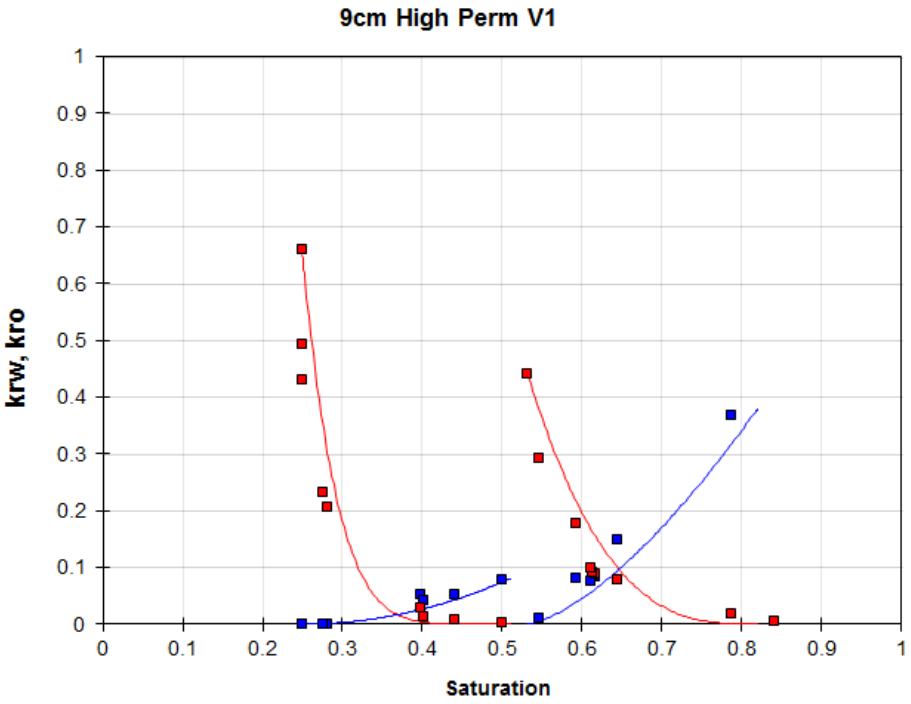

FIGURE 6.4: Relative permeability curves resulting from the JBN analysis of the 7cm production data.

6.4 17cm High Permeability

This set of experiments showed an extremely high degree of reproducibility and this was also seen in the JBN results. The pressure data was also of a very high quality since the lower pressures allowed for a more accurate delta pressure meter, the core also behaved very homogeneously. One of the drawbacks of this is a very instantaneous microemulsion breakthrough which also contained little oil. The absence of a large two phase flow region leaves some empty regions in the relative permeability curves which needed to be interpolated.

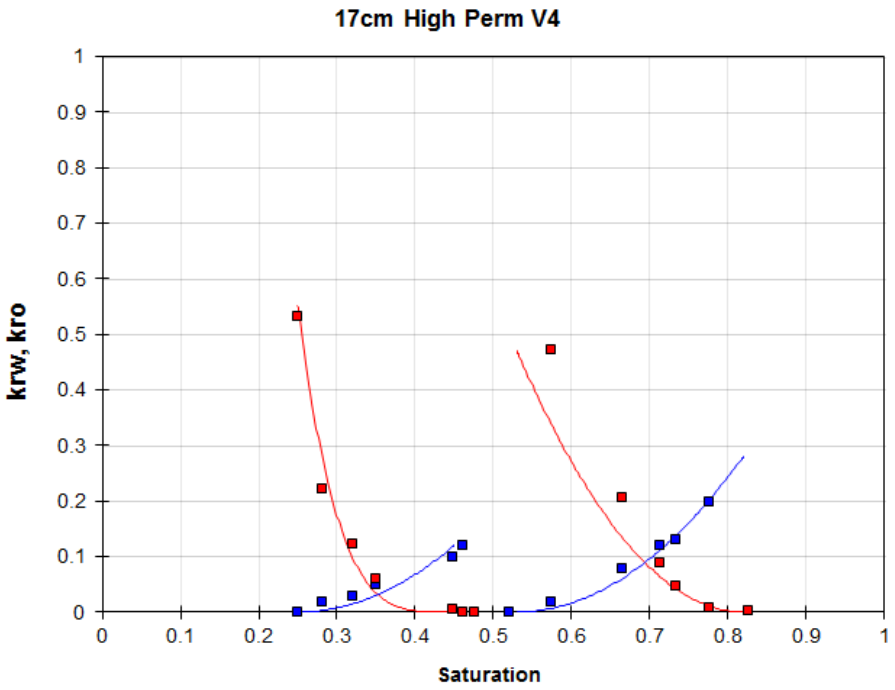

FIGURE 6.5: Relative permeability curves resulting from the JBN analysis of the 17cm production data.

6.5 30cm High Permeability

The last data set only includes experimental data using iodododecane oil. The unstable displacement seen in the production data and pressure data means that the relative permeabilities for the chemical flood are incorrect (Fig. 6.6). The graph is included as an example of an output when displacement is not piston-like, and oil bank not successfully formed.

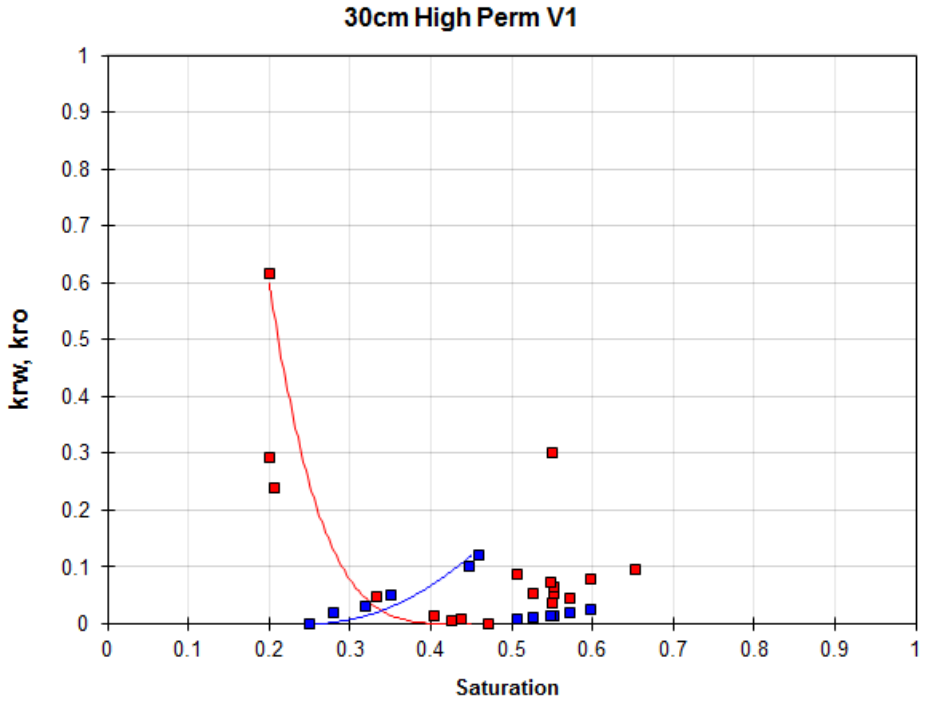

FIGURE 6.6: Incorrect rel perms due to unsteady displacement in the 30cm high permeability cores.

6.6 Discussion

6.6.1 Low Permeability 17 vs 39cm

Setting the curves from both cores side-by-side (Fig. 6.8) we would expect the most prominent confirmation of our hypothesis. The pore volume of the larger length core is almost 200% that of the 17cm core, 33ml and 17ml respectively. What is immediately obvious is the difference in initial oil saturation observed in the production data. Regardless the oil saturation after waterflood is similar in both cases. A big difference can be observed in the oil relative permeability. Not only is the oil bank larger but the oil rel-perms are almost twice as high in the longer length core. This is evidence supporting the hypothesis that given more pore volume, the oil bank is able to coalesce effectively and be transmitted more easily through the core.

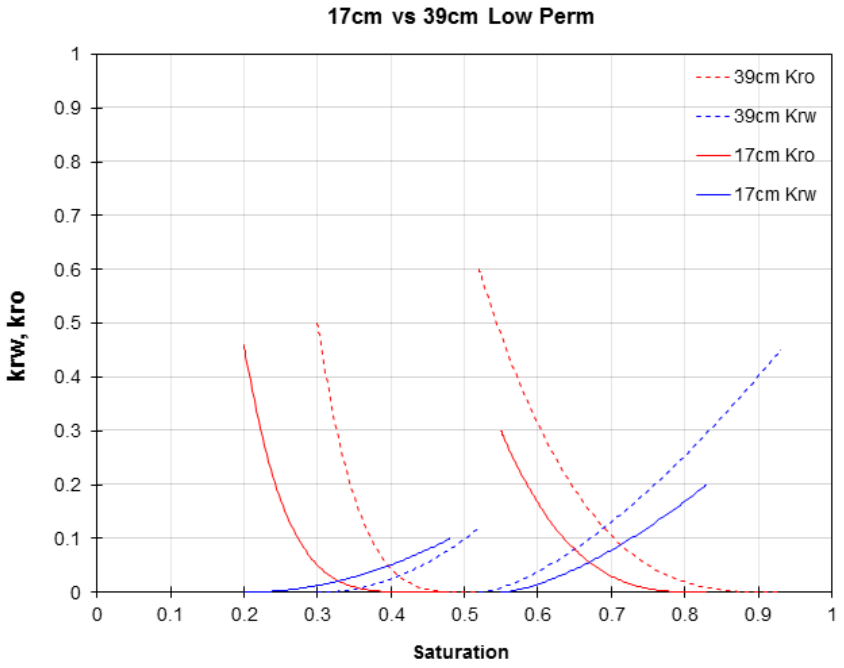

FIGURE 6.7: Comparison of the relative permeability results of the low permeability (solid curves) and the high permeability curves (dotted curves).

6.6.2 High Permeability 7 vs 17cm vs 39cm

The data sets for the two high permeability cores and the 39cm core meet the initial criteria regarding accuracy and reproducibility. Therefore we are also able to make comparisons regarding the differences in rel-perms across core lengths. This is shown in figure 6.8 which overlays the curves over each other. The water flood rel-perms are very similar as expected since rock properties and displacing fluids are the same. The 39cm water flood rel-perms are shifted rightwards since the initial oil saturation for these experiments are lower. During the chemical flood we see a larger shift to the right due to the higher oil bank recovery in the 17cm cores (S_{or} of 0.10 as opposed to 0.13). The oil relative permeabilities are also slightly higher but not to the extent in the low permeability cores. The reason for this is likely two-fold: Firstly

the increase in pore volume is not as dramatic as in the low perm cores. Secondly the homogeneity of the high permeability cores means that the majority of the oil will most likely be mobilised regardless of whether or not an oil bank is formed. As permeability and homogeneity decreases the effectiveness of the surfactant polymer slug to reduce IFT and mobilise residual oil into an oil bank becomes more essential.

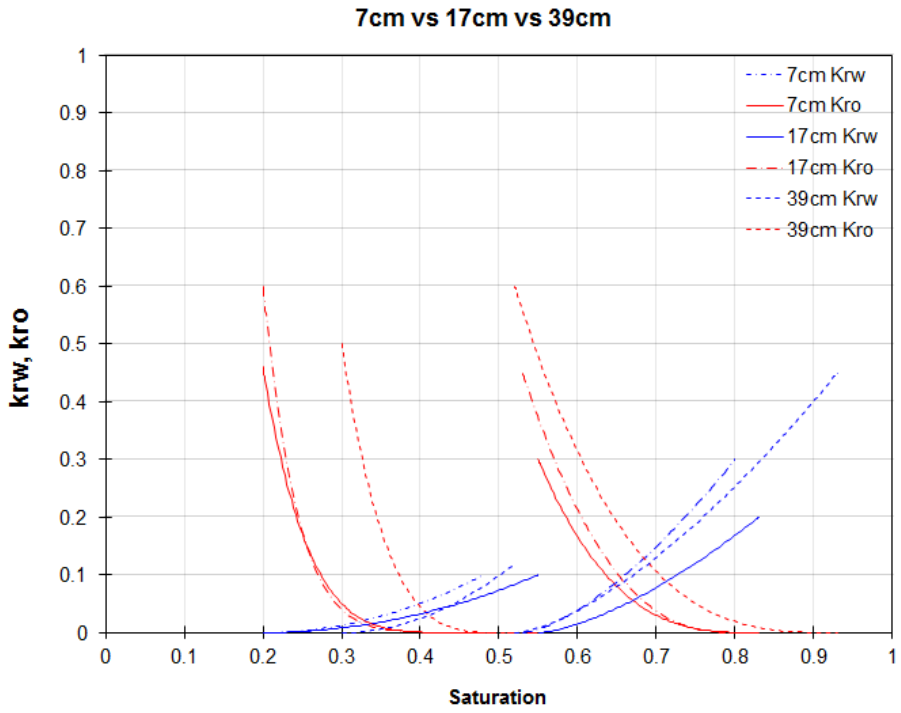

FIGURE 6.8: Comparison of the relative permeability results of the low permeability (solid curves) and the high permeability curves (dotted curves).

6.6.3 High vs. Low Permeability

Similarly the data allows for a comparison of the results of the high and low permeability core-floods. In this case we are not increasing the core length but due to the higher porosity and permeability the pore volume has increased by 40%. Looking at the two curves in figure 6.9 it can be concluded that under similar displacement conditions, the oil is moving more freely most likely due to a larger oil bank.

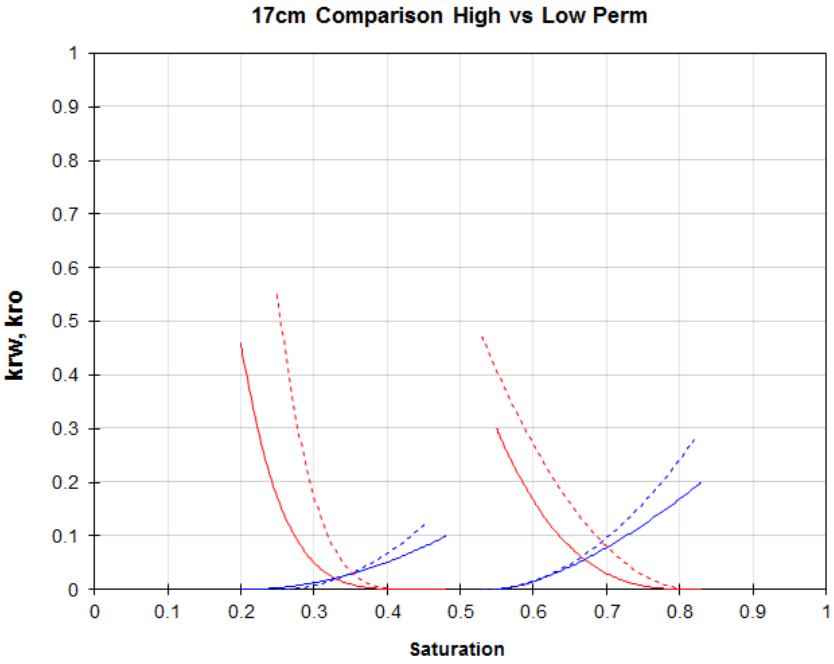

FIGURE 6.9: Comparison of the relative permeability results of the low permeability (solid curves) and the high permeability curves (dotted curves).

Chapter 7

Results: Numerical Simulator

The JBN method is an unsteady-state analytical solution which has a number of inherent uncertainties. Taking into account the uncertainty of the production data it is important to check the accuracy of the analytical results. This can be done by using the data as input parameters for a reservoir simulator. Shell Global's modular reservoir simulator (MoReS) was used to do this. It uses a finite difference scheme where the coupled material balance and flow equations are solved at the centre of the grid points. A model was created that mimics the core properties and set-up used in the experiments. The core flood is then modelled numerically using the analytically derived relative permeabilities from chapter 5. With the first model, Atlas 23, the waterflood and chemical floods are simulated individually. The Atlas 53 model is more extensive and combines the water and chemical flood in one simulation. Comparing the simulated production results to the experimental results gives an idea of how realistic the input parameters are.

7.1 Atlas 23

This model is based on a simple 2D grid representing the core flood set-up. It can model a single sweep of the core with a displacing fluid. To initialise the model the grid parameters and rock properties are defined. Next the injection properties are specified, such as polymer concentration and interfacial tension as measured in the phase behaviour test. The injection rate is stated and finally the user defined two-phase rel-perm and production data is imported. The model simulates an arbitrary number of pore volumes injected and plots the numerical data over the experimental data. A visual representation of the model is given below with the core shown together with an injection point at the bottom and a production point opposing it. The snapshot is taken approximately 30 minutes into the 9cm core flood. This coincides with around a little under half a pore volume of injection which is replicated by the model.

7.1.1 17cm Low Permeability

The following chart (Fig. 7.2) shows the simulated data plotted over experimental data from the 17cm low permeability cores. The cumulative oil recovery over time and the pressure data are shown. Using the JBN rel-perms for the waterflooding stage we see a similar pressure response as in the core flooding experiments. The match will never be perfect since the experimental data contains some irregularities such as the small dip 0.1 hours into the data. The experimental data rarely shows the sharp pressure response which is produced by the simulated flood. From the CT data and production data we see the chemical front is slightly "smeared" which results in some early breakthrough and a flattened pressure response.

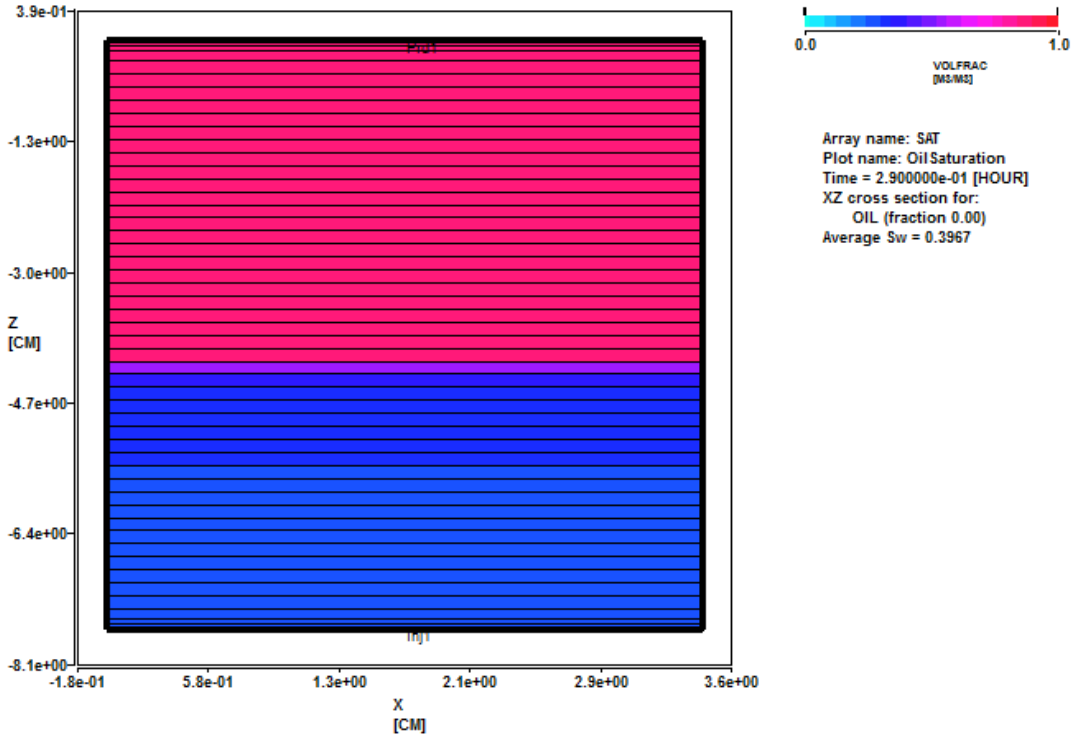

FIGURE 7.1: Simulator grid showing the chemical flood (blue) displacing the oil in the core with the flow characteristics determined by the rock properties and JBN rel-perms.

One interesting observation is that the initial porosity-permeability tests performed on the rock showed a permeability in the order of 10mD. From the data the maximum pressure difference over the core during the chemical flood is almost 40bar. When doing the initial runs of the Atlas 23 model the pressure never reached this order of magnitude, staying in the 5-6bar region. Unfortunately brine permeability testing was not done for these experiments. Using pressure data from the core flushes a retrospective brine permeability test was done. This resulted in permeability values of 1-2mD which is significantly lower than what resulted from the core plugs. Using this new value the simulator pressure data resulted in a much better fit.

A likely explanation for this are heterogeneities in the rock. In a failed experiment using 1m cores an analysis was done using the CT images. The resulting image shown in Appendix E attempts to relate the permeability to the CT numbers from the x-ray attenuation. It can be seen that the first sections of the core fall in the permeability regimes seen in the core plugs tested in the permeameter. The pressure in the subsequent sections was so high that it caused failure of the delta P sensors. Assuming the Houndsfield units are indeed a linear transformation of the attenuation coefficient the permeability in one section approaches 0.5mD. The scale of these variations are in the order of half a meter. It is possible that cores contain similar heterogeneities as seen in the 1m sample which were missed by the plugs due to their scale.

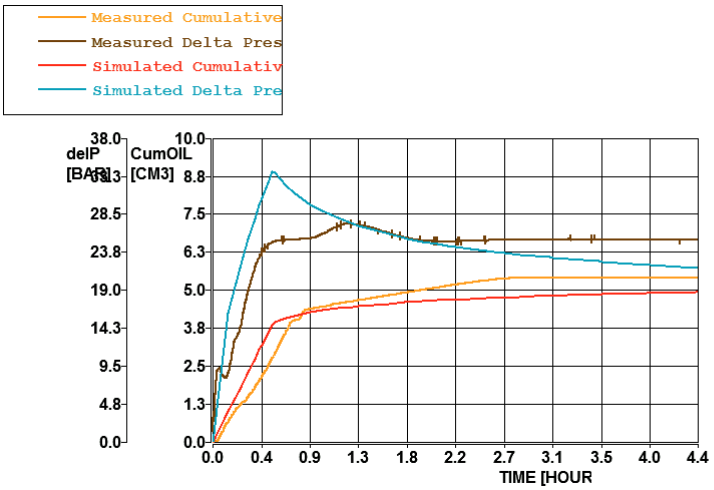

FIGURE 7.2: Comparison of the experimental and analytical pressure and production data for the 17cm LP cores.

7.1.2 39cm Low Permeability

The match for the numerical and analytical data for the 39cm core is relatively good. There is a slight mismatch between the pressure data however this is likely due to poor shifting of the pressure data when correcting for dead volume. The data is being recorded across the core in real time, however the production data is delayed by approximately 0.2PV due to the dead volume between the end of the core and the data recording equipment. The second curves plotted represent the water saturation in the core. Looking at the cumulative oil production a similarly good match can be seen between the two data sets.

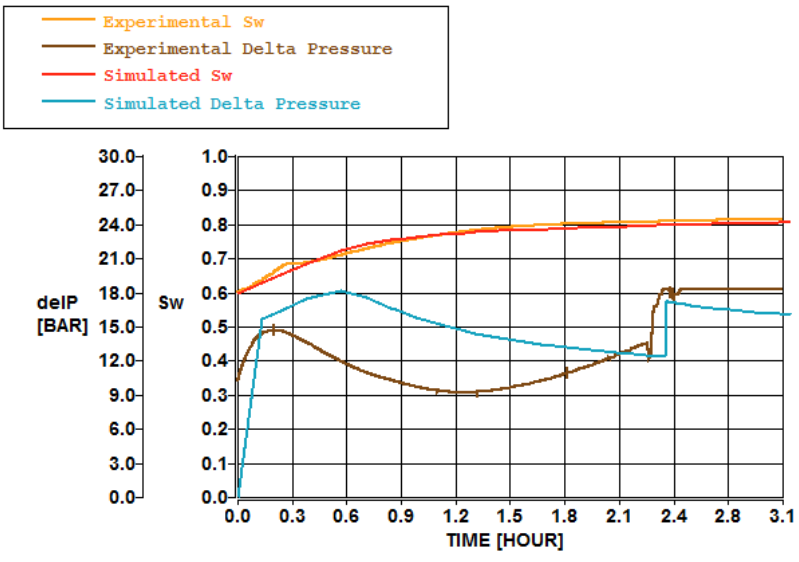

FIGURE 7.3: Comparison of the experimental and analytical pressure and saturation data for the 39cm LP cores.

7.1.3 7cm High Permeability

The JBN rel-perms perform less convincingly for the higher permeability cores. The cumulative oil production is approximately 20% higher in the experimental results. The saturation data seems to fit well however the pressure data match is also poor. This is where we see some of the shortcomings of the Atlas 23 model. It lacks the complexity to accurately model the surfactant polymer slug and the polymer chaser. The chemical flood is treated as a whole with the two components lumped into one displacing fluid with constant properties. This is why it resembles a waterflood with a single pressure spike. In reality the pressure shows a steady increase before oil bank breakthrough, a decrease with the arrival of the surfactant front and a subsequent increase as the polymer is produced.

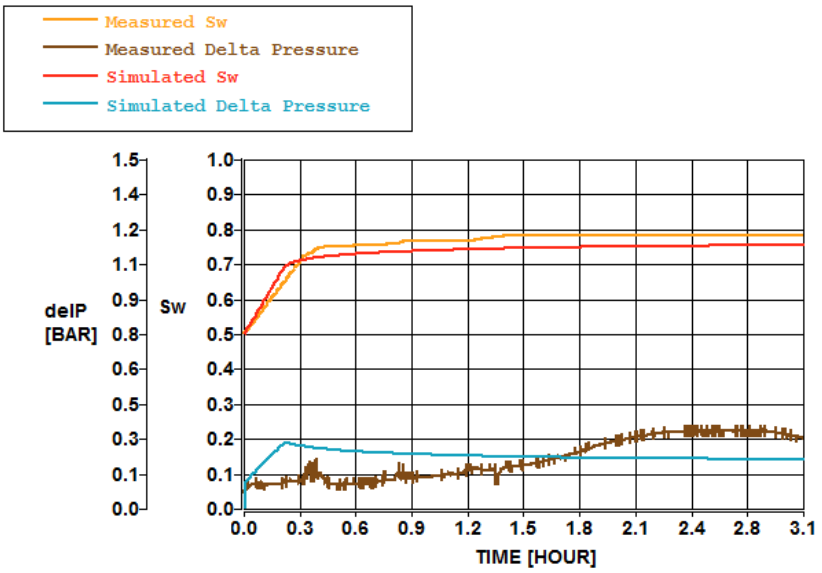

FIGURE 7.4: Comparison of the experimental and analytical pressure and saturation data for the 7cm HP cores.

7.1.4 17cm High Permeability

The final data set fed into the Atlas 23 model is the 17cm cores with higher permeability. Again we fail to get accurate replication of the pressure data. This is due to the reason mentioned in the previous section. The experimental pressure shows the expected build up as the oil bank propagates through the core and the gradual decrease as the microemulsions and surfactant polymer are back produced. Similarly cumulative oil production from the simulator shows an underestimation of approximately 15%.

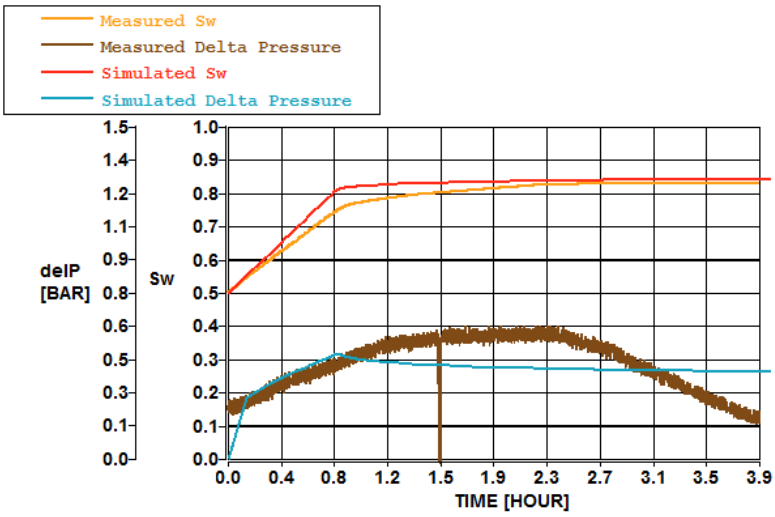

FIGURE 7.5: Comparison of the experimental and analytical pressure and saturation data for the 17cm HP cores.

7.2 Atlas 53

The Atlas 23 model was able to accurately model the waterflood component in each of the experiments using the JBN rel-perms. With some tweaking it also gave a crude estimation of the quality of the chemical rel-perms, however it lacked some essential parameters needed to correctly model this part of the flood. Therefore it was chosen to use the Atlas 53 model. This is more complex model designed for a variety of core flood models. It uses passive tracers to model the chemical components which is less computationally intensive and simplifies the history-matching process. The model captures the following chemical processes:

1. Interfacial tension (IFT) lowering due to the presence of soap and surfactant. Salinity effects on the IFT are also captured.
2. Desaturation of the oil saturation below the residual to water flood due to increased capillary number.
3. Polymer viscosity modelling. Impact of polymer concentration, salinity, shear rate and resistance factor on polymer mobility are taken into account.
4. Polymer hydrodynamic acceleration
5. Adsorption of chemicals

The 3D model and accompanying grid is shown in Figure 7.6 below:

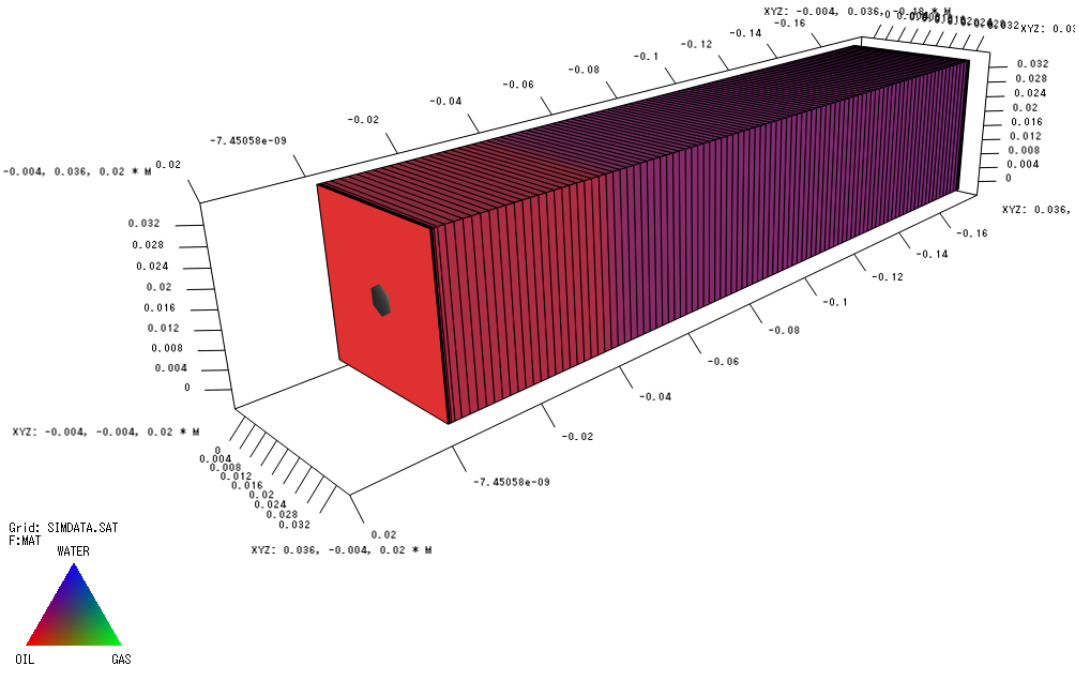

FIGURE 7.6: The 3D grid used in the Atlas 53 model.

A number of these parameters (polymer mobility effects and saponification) go beyond the scope of the research project and will therefore be disabled in the model. Although this is already a big step forward the model still has some short-comings.

1. No modelling of the micro-emulsion phase.

2. All chemicals remain in the aqueous phase, no partitioning or interactions.
3. No modelling of the (geo)chemistry.
4. Capillary pressures are largely negelected however imbibition curves can be incorporated.

The model allows for specification of the individual SP and polymer characteristics. Surfactant concentrations and the resulting IFT are all taken into account as well as polymer viscosities and salinity effects. In the resulting visualisation we are able to see the two phase displacement during the waterflood. And even oil bank formation in the model, where a front of higher oil concentration is seen preceding the SP front.

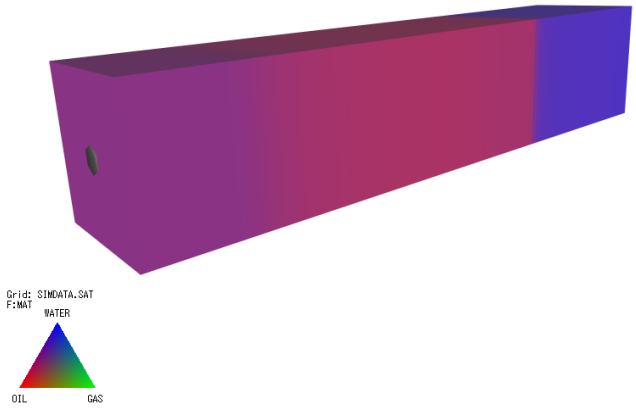

FIGURE 7.7: Snapshot taken during the chemical flood with a region of higher oil concentration seen preceding the surfactant polymer front.

7.2.1 17cm Low Permeability

Below is the result of the complete modelling of the 17cm low permeability core flood. After initial saturation the model is flooded with water until no more oil is produced. This is followed by a chemical flood of 0.5PV of surfactant polymer and a polymer chaser of 1PV. The flow characteristics are determined by the JBN relative permeabilities determined in chapter 5.

The two data sets match very closely with the majority of the difference coming from the effect of the inhomogeneities in the core. There is some degree of two-layer flow seen in both the water- and the chemical-flood. The preferential flow through one of the layers results in a subtle two-step response in oil production which is not seen in the model data. Incorporating two separate layers in the model would result in similar behaviour. The match in pressure data is not as good. The biggest differences are intentional due to large increases in flow rate during the experiment to speed up the flushing process (seen @ 1.1 and 5.2PV). The linear decline in the model after polymer breakthrough seems unrealistic.

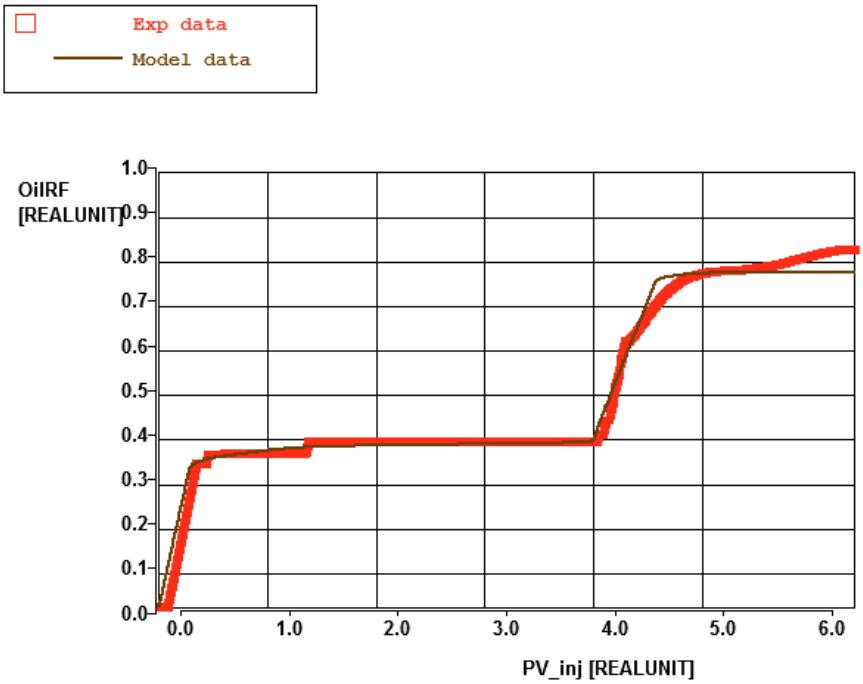

FIGURE 7.8: Match of the experimental production data and the results of the Atlas 53 model.

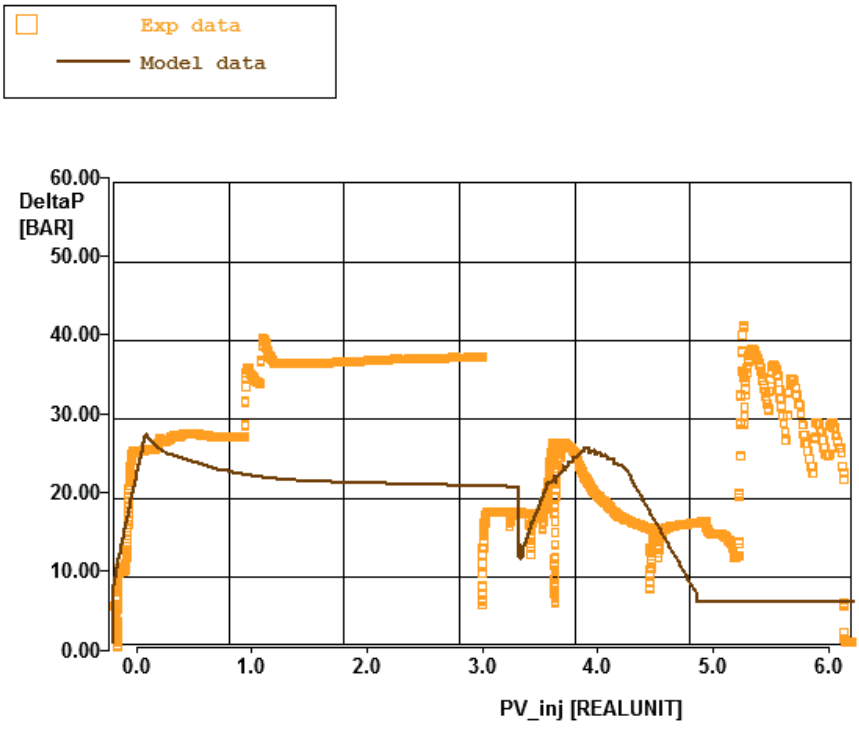

FIGURE 7.9: Match of the experimental pressure data and the results of the Atlas 53 model.

7.2.2 7cm High Permeability

Using the JBN rel-perms for the 9cm cores resulted in an overestimation of the oil recovery and a mismatch in pressure. This means that the relative permeabilities from the JBN method were too optimistic and would explain why little difference was seen between the 7 and 17cm JBN results. Tuning down the rel-perms resulted in a much better fit of the production and pressure data, see figures 7.12 and **??**.

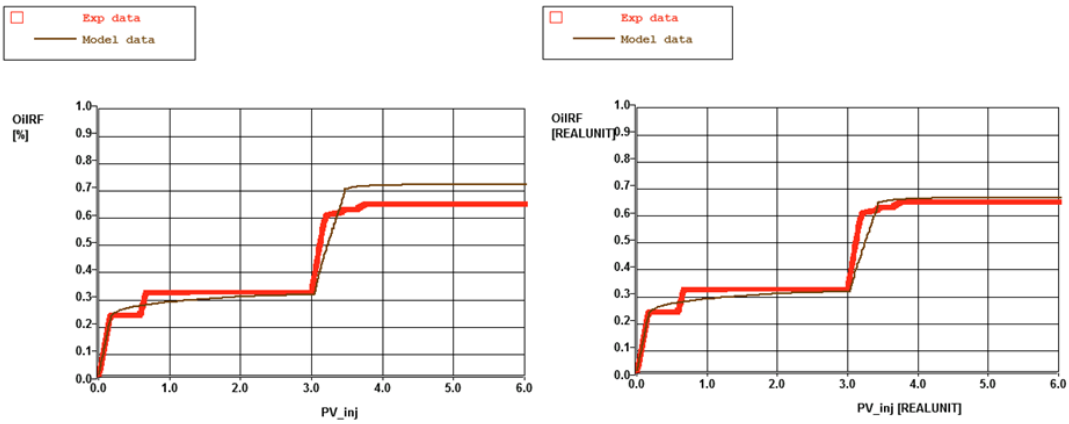

FIGURE 7.10: Match of the 7cm high perm experimental and Atlas 53 numerical production data, before and after tuning the rel-perms.

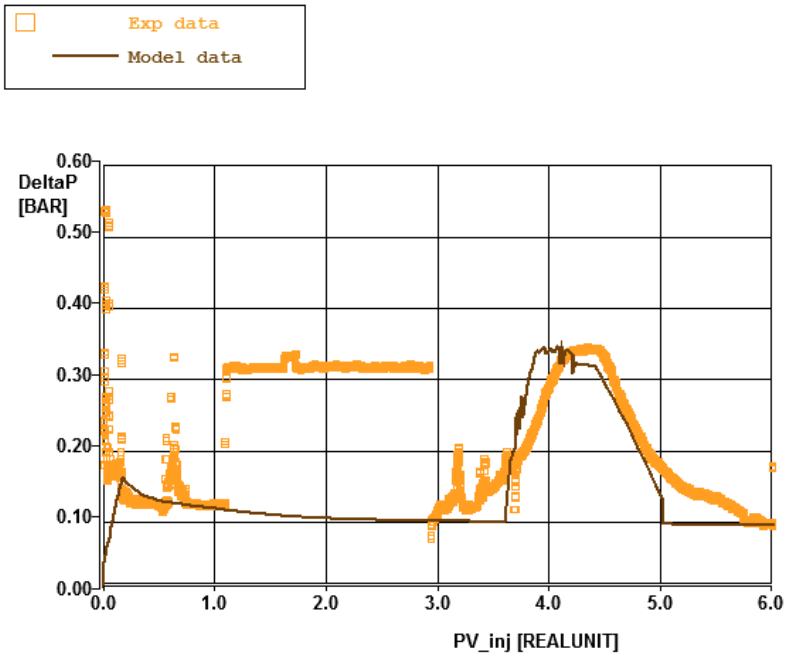

FIGURE 7.11: Match of the experimental pressure data and the results of the Atlas 53 model for the 7cm high perm core-flood.

7.2.3 17cm High Permeability

The final data set tested using the Atlas 53 model is the 17cm high permeability cores. Comparing the numerical results this match is the closest of all the runs. These cores showed the lowest degree of heterogeneity and very good reproducibility. This means that the homogeneous model used comes very close to the ideal displacement simulated.

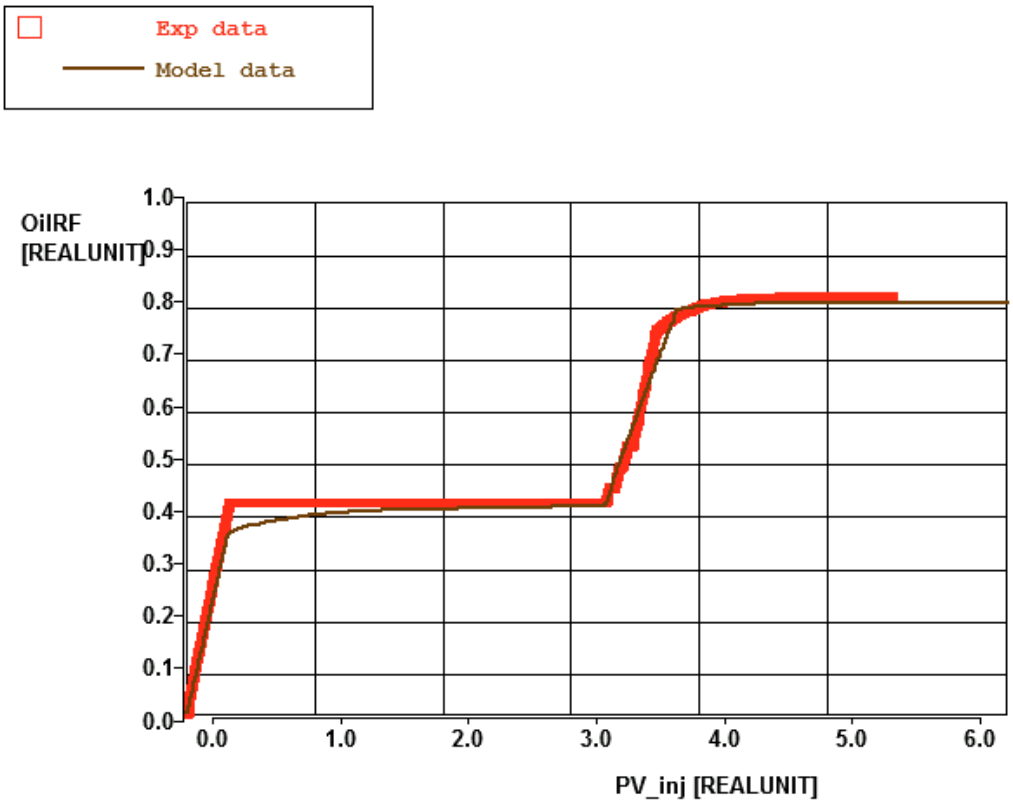

FIGURE 7.12: Match of the 9cm high perm experimental production data and the results of the Atlas 53 model, before and after tuning the rel-perms.

Chapter 8

Conclusions

A core flood set-up was used to investigate oil bank formation in a dodecane system by surfactant polymer injection. Data from these experiments was then used as input for an analytical JBN relperm analysis, who's accuracy was then tested in a numerical simulator. Recalling the initial research objectives, starting with determining the optimum phase behaviour of the chosen surfactant/dodecane system.

- The microemulsions formed during the phase behaviour tests exhibited ultra-low interfacial tension values needed to increase capillary number and mobilise residual oil.

The second objective was whether or not oil bank formation could be observed in all lengths of cores. The hypothesis being that the longer length cores (read larger pore volume) would form a more defined and effective oil bank. Two important success criteria were the robustness of the set-up and reproducibility of the results.

- Core flood experiments using n-dodecane showed successful oil bank formation at core lengths 7, 17, 30 and 39cm, at both low and high permeabilities. Cumulative recovery factors for low permeable samples averaged 80% and high permeable samples 85-90%.
- Longer core lengths lead to larger relative oil banks however they are preceded by a region of slug flow as seen in other research (Batenburg et al., 2015).
- At higher permeabilities the waterflood recovery factor is significantly higher and the oil bank is less defined. This points to a potential relationship between residual oil saturation and oil bank formation.
- Reduction of surfactant polymer slug size from 0.3PV to 0.5PV showed no significant effect on the effectiveness of the sweep or oil bank formation and size in the high permeability cores. In the low permeability cores the smaller slug size resulted in a 20% lower recovery from the chemical flood leaving a residual oil saturation of 0.2. The oil bank was also smaller with a relatively greater production of microemulsions. This suggests that the effect of reducing the slug size is a function of the heterogeneity of the cores.
- All core flooding experiments showed reproducibility in successive experiments. The differences seen were within the uncertainties of the set-up and large differences were caused by user error (ex. poor storage of the surfactant polymer solution). Tracer data showed minimal decrease in accessible pore volume during a series of experiments however brine permeability was reduced by approximately 10% during every run. This is likely due to do polymer deposition during flooding or cleaning with IPA (which is known to dehydrate solutions).

- Experiments performed in the CT scanner using iodododecane gave insight into the displacement processes happening during the core flood. In a number of experiments oil bank formation was not successful. Unstable displacement at the oil/SP interface led to viscous fingering seen on the scans and early breakthrough followed by slug flow observed in the production data. In two of the experiments oil bank formation and propagation was seen.

The final objective was whether or not the production and pressure data could be successfully be interpreted into relperms using the JBN method. Criteria for success was checking the results by inputting them into a tried and tested reservoir simulator. The following conclusions can be made in this regard:

- The JBN emthod was successfully applied to waterflood (as expected) but also to chemical flooding data. For smaller cores with immediate oil bank production the original model can be applied as-is. For longer cores where the oil bank can be characterised by slug flow preceding the bank an alteration should be made. In these cases the slug flow and the oil bank should be analysed separately. The slug flow contributes to incremental oil production from surfactant polymer but should be ignored for the chemical relperm analysis.

- We modify the method by applying it only when solid oil bank is seen, shifting the pressure data to match breakthrough and extrapolating pressure before the oil bank since the slug flow leads to large fluctuations. Using this approach chemical relperms can be determined for the longer core lengths too.

- A second implication is that during this slug flow the majority of the core is still under waterflood relative permeability conditions. The surfactant polymer has only just entered the core and although it is mobilising oil in this region it is also displacing brine in front of it. The flow preceding the front is still dictated by waterflood relative permeabilities. In reality the system transitions from waterflood to chemical relperms over the course of the flood. This is one of the aspects the Atlas 53 deck attempts to model.

- From the resulting curves comparisons can be made between core lengths and permeabilities. With identical displacement processes the surfactant polymer mobilises oil more freely in cores with higher pore volume. Relative permeabilities for the 39cm low perm cores are higher at similar saturations than for the 17cm cores and the same trend is seen to a lesser degree in the high permeability cores.

The JBN rel-perm curves were fed into numerical simulator to test their accuracy. While the simplified Atlas 23 deck showed that the JBN curves were a reasonable estimation, the more complex model confirmed that the relative permeabilities led to a very close match with the simulated production data. The relative permeabilities for the 9cm high permeability cores were overestimated. Any further mismatches were the result of inhomogeneities in the cores.

Chapter 9

Recommendations

Based on the performed experiments and analysis of the data the following recommendations and areas of further research can be made:

- There is still a lot of uncertainty with regards to the nature of phase behaviour. The salinity scan used to determine the optimum is a static process whereas the core floods are dynamic. One can ask whether the results from the phase behaviour test (waiting two weeks for equilibration) is representative of the core flood processes occurring over a matter of hours.
- Research should also be done into the phase behaviour and displacement processes involving iododododecane. It was shown that the oil has a different phase behaviour than dodecane and based on the production and CT data it results in an unstable interaction with the surfactant polymer even at favourable mobility ratios.
- Effect of polymer on the phase behaviour of the systems. In this research they were not included in the study however from literature it is known they often do not solubise in the microemulsion. It is possible, for example, that the polymer in the iododododecane system came out of solution which led to unfavourable mobility.
- More experiments should be done using smaller slug sizes. For this system there will be a lower bound where the lack of volume causes the front to break down.
- Similarly more sensitivities are needed for injection at underoptimum conditions. The limited number of experiments in this research showed proportionally more oil produced in the oil bank with less oil-in-microemulsion. Recovery-wise this seems less effective however there are other advantages which are not taken into account. Such as the increased solubility and more less surfactant precipitation as a result of divalent electrons.
- Analysis of the effluent would be helpful in understanding the microemulsions formed in the core. Due to the high SBA concentration we assume no viscous phase was formed however this could still be the case.
- Performing the same experiments with "non-ideal" systems using crude oil.
- Splitting the core up into multiple regions and performing JBN analysis on these sections to capture the transition from waterflood to chemical relperm conditions.

- The JBN method assumes negligible capillary pressure, but this is still an important aspect of the core floods. This is likely one of the contributors for the remaining mismatches between the Atlas 53 simulations and the experimental data.

Appendix A

Phase Behaviour

This appendix contains the iodododecane salinity scan results as well as some extra observations on the phase behaviour equilibration times.

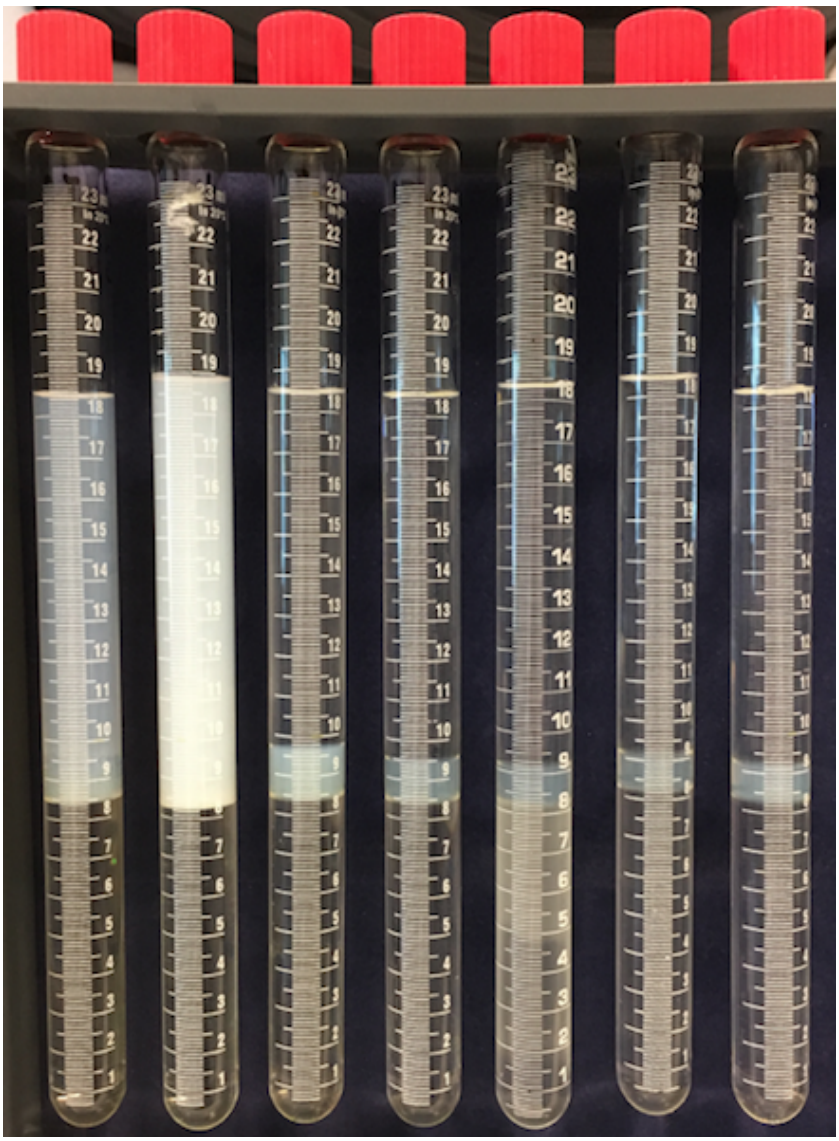

FIGURE A.1: Phase behaviour of the dodecane-oil system using 1% O242 surfactant and 4% SBA as co-solvent. Salinties of the tubes are 3,4,4.25,4.5,4.75,5,6, respectively

As mentioned the salinity scan is based on static system where the test tubes have been allowed to rest and equilibrate for a number of days and sometimes weeks. The core flooding experiments on the other hand are dynamic systems where the oil and surfactant polymer solution are constantly interacting. This mismatch is important to note since it raises the question whether or not the phase behaviour tests are representative of the situation in the core. To get a rough understanding the equilibration was monitored in the minutes and hours after agitation. The results can be found below

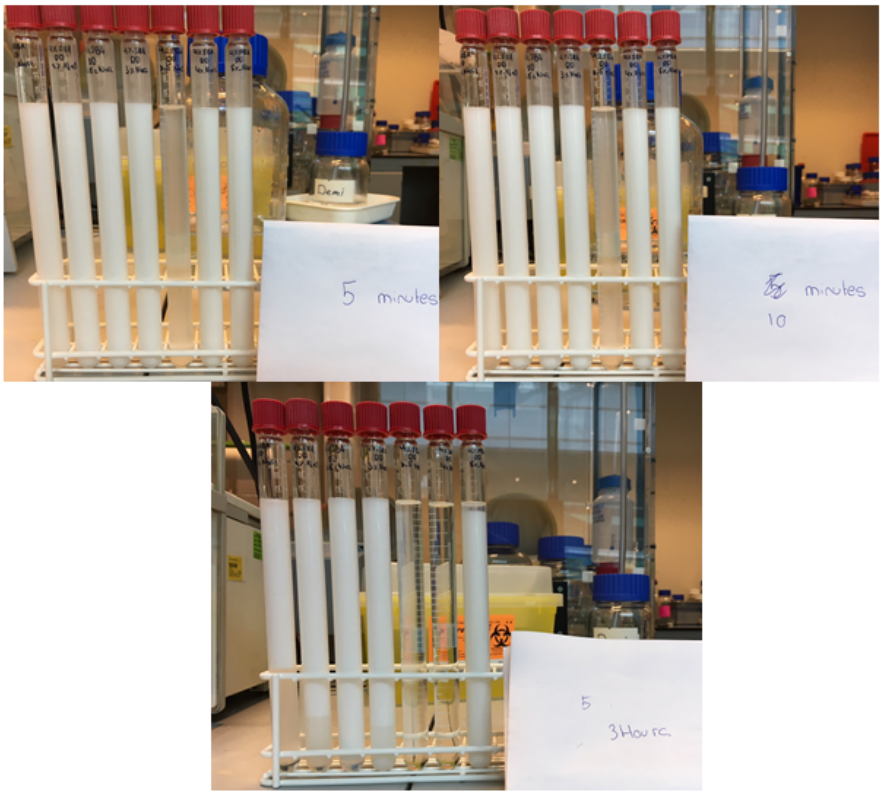

FIGURE A.2: Equilibration of the dodecane phase behaviour test. The tubes were agitated for 60 seconds and then left to settle. Photos were taken every 5 minutes intitially and every hour afterwards.

The takeaway from this is that the equilibration time for the optimum phase behaviour occurs within the first 5 minutes. In the first picture the micro-emulsion phase is already visible and almost at its maximum volume. The core floods occur in a time frame of hours and it is therefore a welcome confirmation that the micro-emulsions are able to form well within this. Unfortunately the same images were not recorded for the iododododecane systems however from conducting the experiments memory recalls that it was nowhere near as fast for equilibration. This might be a contributing factor to the poor performance of the iododododecane core floods.

Appendix B

Surfactant-Polymer Viscosities

Polymer and surfactant polymer viscosities were recorded using the rheometer as mentioned in Chapter 3. The output report is given below and show that the solutions meet the required conditions of $\pm$10cP for the surfactant polymer and a polymer viscosity 25% higher at $\pm$15cP. This will ensure favourable mobility of each respective front.

Report

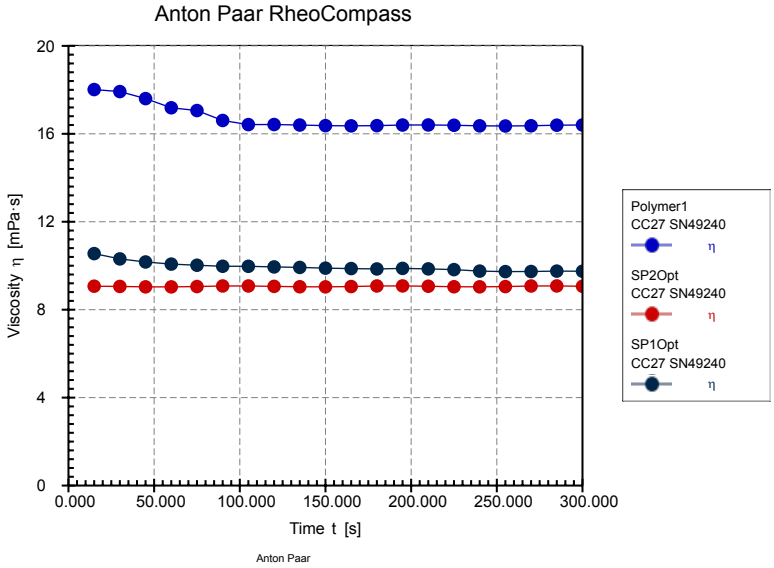

SP1Opt, Shear test, Interval 1

Point No.	Time	Shear Rate	Shear Stress	Viscosity	Torque	Status
№	t	$\dot{\gamma}$	τ	η	M	Stat
	[s]	[1/s]	[Pa]	[mPa·s]	[mN·m]	
1	15.0	6	0.063291	10.551	0.0033609	Dy_auto
2	30.0	6	0.061847	10.31	0.0032842	Dy_auto
3	45.0	6	0.061017	10.17	0.0032401	Dy_auto
4	60.0	6	0.06044	10.074	0.0032095	Dy_auto
5	75.0	6	0.060128	10.021	0.0031929	Dy_auto
6	90.0	6	0.05985	9.975	0.0031781	Dy_auto
7	105.0	6	0.05984	9.9734	0.0031776	Dy_auto
8	120.0	6	0.059672	9.9454	0.0031687	Dy_auto
9	135.0	6	0.059536	9.9226	0.0031615	Dy_auto
10	150.0	6	0.059332	9.8886	0.0031506	Dy_auto
11	165.0	6	0.059219	9.8698	0.0031446	Dy_auto
12	180.0	6	0.059112	9.8521	0.003139	Dy_auto
13	195.0	6	0.059268	9.8781	0.0031473	Dy_auto
14	210.0	6	0.059131	9.8553	0.00314	Dy_auto

Anton Paar

FIGURE B.1: Viscosity of the surfactant polymer (black/red) and the polymer (blue). Tests were done at room temperature and a constant shear rate of 6 [$1/\dot{\gamma}$]

Appendix C

Tracer Analysis

An example of a tracer analysis result is given below. This is from the 9cm high permeability data set. The most important aspect of the tracer analysis is to see whether or not the accessible pore volume of the core is affected by subsequent runs. As oil is injected and the core is waterflooded the dispersion curve shifts to the left indicating a loss in pore volume since this is now occupied by residual oil. After chemical flooding the curve shifts back to the right since more oil is produced. Cleaning the curve afterwards should bring it back to its initial postition. Polymer deposition, viscous phase from the microemulsions, dislodged grains and solution contaminations can all block the pore throats leading to restricted flow. This will show up as a reduction in accessible pore volume in the tracer analysis. In most experiments there was an initial loss in pore volume after the first run. Afterwards however the tracer analysis showed that cleaning with isopropanol consistently brought the pore volume back to its initial state.

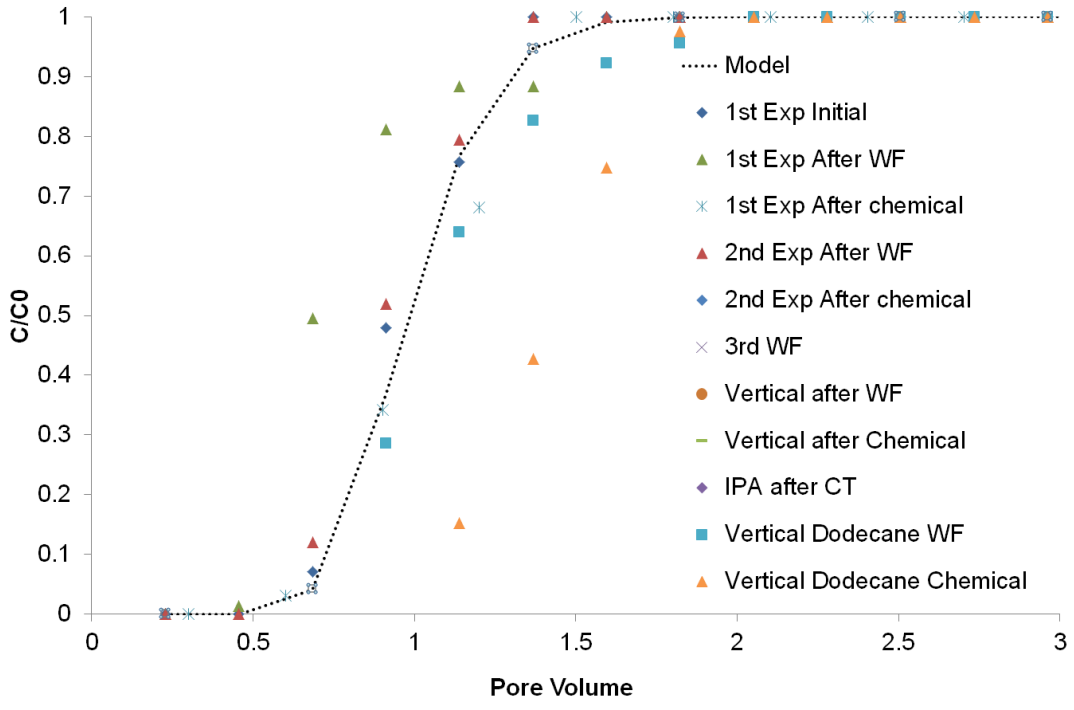

FIGURE C.1: Example of one set of tracer results from the 9cm high permeability experiments. Reduction in accessible pore volume, due to residual oil and/or contamination is represented as a shift to the right. Cleaning with IPA shifts the curve back rightward indicating a return to initial conditions.

Appendix D

Pressure Data - 30cm Chemical Flood

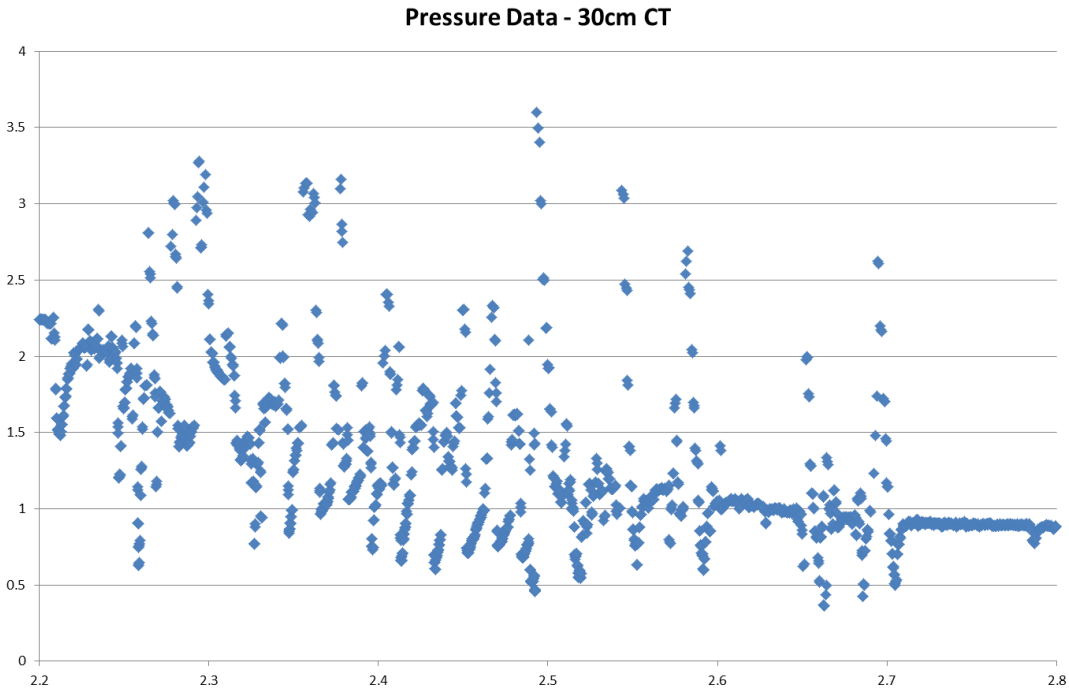

FIGURE D.1: The pressure data from the 30cm chemical core flood experiment. The unstable flow results in constant slug flow and erratic pressure data. This is the reason the data set could not be analysed further.

Appendix E

Analysis - 1m Low Perm. Cores

After seeing a pressure drop along the core that was much greater than expected the CT images were analysed in an attempt to get an idea of the permeabilities in the core. Since DP meters were placed along 10cm intervals along the core we knew the permeabilities in the first four sections of the core. Beyond this the pressure drop become so great that the meters failed. The average value of the Houndsfield (HF) units was calculated along every CT slice and plotted as the blue line over the scan itself. The general trend is similar to what was seen in the pressure drop, which became greater over each subsequent section. Beyond section 5 the density increases even more and if we assume a linear relationship in HF and permeability, the 8th and 9th sections approach sub-1mD permeabilities. These permeability variations are the reason these experiments failed and why the simulator results for the 17cm LP cores gave different results.

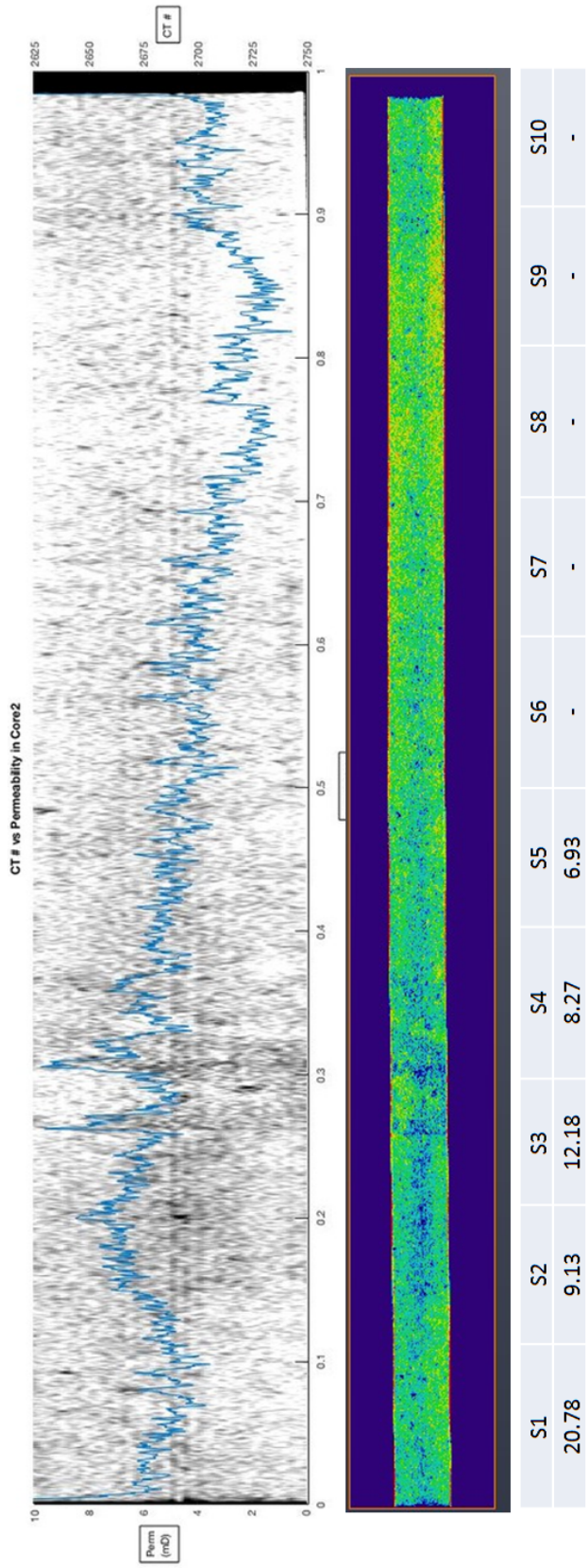

FIGURE E.1: Attempting to relate CT scan (Houndsfield Units) to the permeability along the core length.

Bibliography

Abrams, A (1975). "The Influence of Fluid Viscosity, Interfacial Tension, and Flow Velocity on Residual Oil Saturation Left by Waterflood". In: *Society of Petroleum Engineers Journal* 15.05, pp. 437–447. ISSN: 0197-7520. DOI: 10.2118/5050-PA. URL: http://www.onepetro.org/doi/10.2118/5050-PA.

Barnes, Julian R et al. (2010). "Application of internal olefin sulfonates and other surfactants to eor . part 1 : structure - performance relationships for selection at different reservoir conditions". In: *Society of Petroleum Engineers*, pp. 1–16. DOI: 10.2118/129766-MS.

Batenburg, D W van et al. (2015). *Visualisation of Light Oil Mobilisation in ASP Core Floods Using X-Ray CT Imaging*. Kuala Lumpur, Malaysia. DOI: 10.2118/174660-MS.

BP (2018). "BP Energy Outlook Energy 2018". In: *BP Statistical Review of World Energy*, p. 52. ISSN: 1098-6596. DOI: 10.1017/CBO9781107415324.004. URL: https://www.bp.com/content/dam/bp/pdf/energy-economics/energy-outlook-2017/bp-energy-outlook-2017.pdf.

Brownell, L.E. and D.L. Katz (1947). "Flow of Fluids Through Porous Media—Part II". In: *Chem. Eng. Prog.* 43.11, p. 601.

Buckley, S and M Leverett (1942). "Mechanism of fluid displacement in sands". In: *Trans. AIME* 146.1337, pp. 107–116. ISSN: 0081-1696. DOI: 10.2118/942107-G. URL: http://www.onepetro.org/mslib/app/Preview.do?paperNumber=SPE-942107-G&societyCode=SPE%5Cnhttp://scholar.google.com/scholar?hl=en&btnG=Search&q=intitle:Mechanism+of+Fluid+Displacement+in+Sands#0.

Delshad, M et al. (1986). "Effect of Capillary Number on the Residual Saturation of a Three-Phase Micellar Solution". In: *SPE Enhanced Oil Recovery Symposium*. DOI: 10.2118/14911-MS. URL: http://www.onepetro.org/mslib/app/Preview.do?paperNumber=00014911&societyCode=SPE.

Falls, a.H. et al. (1994). *Field Test of Cosurfactant-Enhanced Alkaline Flooding*. DOI: 10.2118/24117-PA.

Goddard, E.D. (1989). "Surfactants and interfacial phenomena". In: *Colloids and Surfaces* 40, p. 347. ISSN: 01666622. DOI: 10.1016/0166-6622(89)80030-7. URL: http://linkinghub.elsevier.com/retrieve/pii/0166662289800307.

Hirasaki, George and Danhua Leslie Zhang (2004). "Surface Chemistry of Oil Recovery From Fractured, Oil-Wet, Carbonate Formations". In: *SPE Journal* 9.02, pp. 151–162. ISSN: 1086-055X. DOI: 10.2118/88365-PA. URL: http://www.onepetro.org/doi/10.2118/88365-PA.

Holmes, David W. et al. (2016). "Characterizing flow in oil reservoir rock using SPH: absolute permeability". In: *Computational Particle Mechanics* 3.2, pp. 141–154. ISSN: 21964386. DOI: 10.1007/s40571-015-0038-7.

Homsy, G M (1988). "Interfacial Phenomena: Equilibrium and Dynamic Effects. By C. A. MILLER and P. NEOGI. Dekker, 1985. 354 pp." In: *Journal of Fluid Mechanics* 187, pp. 598–599. ISSN: 0022-1120. DOI: DOI:10.1017/S0022112088220584. URL: https://www.cambridge.org/core/article/interfacial-phenomena-equilibrium-and-dynamic-effects-by-c-a-miller-and-p-neogi-dekker-1985-354-pp-6950/CA09E574F2F056DFC03FFEEB9A3A5B76.

Johnson, E. F., D. P. Bossler, and V. O. Naumann (1959). "Calculation of relative permeability from Displacement Experiments". In: *Petroleum Transactions, AIME*, pp. 370–372. DOI: 10.2118/1023-G.

Miller C, Neog P (1986). "INTERFACIAL PHENOMENA (Equilibrium and Dynamic Effects)". In: *Journal of Dispersion Science and Technology* 7.1, pp. 127–128. ISSN: 0193-2691. DOI: 10.1080/01932698608943452. URL: https://doi.org/10.1080/01932698608943452.

Morrow, N R and B Songkran (1981). "Effect of viscous and buoyancy forces on nonwetting phase trapping in porous media". In: *Surface phenomena in enhanced oil recovery*. Springer, pp. 387–411.

Pope, G.a. Gary A. and R.C. C. Nelson (1978). "A Chemical Flooding Compositional Simulator". In: *Society of Petroleum Engineers Journal*. ISSN: 0197-7520. DOI: 10.2118/6725-PA.

Rosen, M J and J T Kunjappu (2012). "Surfactants and Interfacial Phenomena, 4th Edition". In: *Surfactants and Interfacial Phenomena, 4th Edition*, pp. 1–122. ISBN: 978-1-118-22893-7; 978-0-470-54194-4. DOI: 10.1002/9781118228920.

Saadi, Faisal Al (2017). "Fontainebleau Sandstone". In:

Sahni, Vinay et al. (2010). "The role of co-solvents and co-surfactants in making chemical floods robust". In: *Spe 130007* 1976. DOI: 10.2118/130007-MS.

Sanz, C. and G. Pope (1995). "Alcohol-Free Chemical Flooding: From Surfactant Screening to Coreflood Design". In: *Proceedings of SPE International Symposium on Oilfield Chemistry*, pp. 117–128. DOI: 10.2523/28956-MS. URL: http://www.spe.org/elibrary/servlet/spepreview?id=00028956.

Vonnegut, Bernard (1942). "Rotating bubble method for the determination of surface and interfacial tensions". In: *Review of Scientific Instruments* 13.1, pp. 6–9. ISSN: 00346748. DOI: 10.1063/1.1769937.

Welge, Henry J. (1952). "A Simplified Method for Computing Oil Recovery by Gas or Water Drive". In: *Journal of Petroleum Technology* 4.04, pp. 91–98. ISSN: 0149-2136. DOI: 10.2118/124-G. URL: http://www.onepetro.org/doi/10.2118/124-G.

Winsor, P. A. (1948). "Hydrotropy, solubilisation and related emulsification processes". In: *Transactions of the Faraday Society* 44, p. 376. ISSN: 0014-7672. DOI: 10.1039/tf9484400376. URL: http://xlink.rsc.org/?DOI=tf9484400376.

Zolotukhin, Anatoly B and Jann-Rune. Ursin (2000). *Introduction to petroleum reservoir engineering*. English. Kristiansand, Norway: Høyskoleforlaget, Norwegian Academic Press. ISBN: 8276340652 9788276340655.